ΕΛΛΗΝΙΚΗ ΔΗΜΟΚΡΑΤΙΑ
Εθνικό και Καποδιστριακό Πανεπιστήμιο Αθηνών

ΠΤΥΧΙΑΚΗ ΕΡΓΑΣΙΑ

Η κατανομή της Can1 στα εισοσώματα και ο ρόλος της ως μηχανισμός ρύθμισης

Στυλιανός Γκιώνης

Α.Μ. 1113201100024

ΕΠΙΒΛΕΠΩΝ
Καθ. Γιώργος Διαλλινάς

ΣΥΝΕΠΙΒΛΕΠΩΝ
Δρ. Χρήστος Γουρνάς

ΤΜΗΜΑ ΒΙΟΛΟΓΙΑΣ

ΑΘΗΝΑ

2018

HELLENIC REPUBLIC
National and Kapodistrian University of Athens

UNDERGRADUATE THESIS

Conformation dependent partitioning of Can1 into starvation protective domains

Stylianos Gkionis

Reg. No. 1113201100024

SUPERVISOR
Prof. George Diallinas

COSUPERVISOR
Dr. Christos Gournas

DEPARTMENT OF BIOLOGY

ATHENS

2018

Acknowledgments

I would like to express my gratitude to Prof. Bruno André for accepting me in his lab, for his guidance and for his continuing support, even after the completion of this project. To all the members of the lab, a big thank you, for the friendly and at the same time stimulating environment that made my stay in Belgium a delight.

To my co-supervisor, Dr. Christos Gournas, who became a friend, for his untiring assistance, for his guidance in all matters, professional, scientific, or personal and foremost for his patience and mentoring with me from the outset, my gratitude as well.

I am of course indebted to Prof. George Diallinas for believing in me and impelling me repeatedly to follow my interests.

I can but mention my teachers Prof D. S. and M. A. for being the guiding compasses in many decisions in my life.

Friends and family, peace out.

Table of Contents

1. Abstract

The plasma membrane of yeast has been shown to be highly compartmentalized, composed of numerous, overlapping domains. While it is known that some membrane proteins dynamically localize between compartments, little information is available regarding the factors affecting this dynamic behavior or its physiological significance. This thesis focuses on one such protein, Can1, the arginine permease of yeast, which preferentially clusters in EMCs but is also found in other compartments. Using confocal laser microscopy, the degree of this enrichment was quantified to show that it depends on the activity and conformation of the transporter, while being independent of its ubiquitination status. Complex sphingolipids appear to play an essential role, as inhibition of the relevant biosynthesis pathway results in the extinction of the phenomenon. By integrating previous observations in the field, a mechanistic model thus emerges for the localization behavior of Can1, as well as a possible function of EMC/eisosomes in general.

2. Introduction

2.1. The Plasma Membrane and its Organization

The plasma membrane serves a multitude of roles. It is the defining boundary of the cell and as such, an important point of regulation for the intake and export of all substances. Most signaling, environment sensing and cell-to-cell communication requires receptors or other components residing there. Cell wall biosynthesis and remodeling is facilitated by the mechanisms of endo- and exocytosis, which also serve other purposes. Indicative of its importance is the fact that it is the target of most pharmaceutical drugs. To achieve all these dynamic roles, a high degree of organization and specialization is required. In recent years it has become evident that, the plasma membrane is not as homogenous as previously thought and that the relationships between its components are dynamic and related to their function. The classical fluid-mosaic model of the lipid bilayer interspersed with integral membrane proteins (Singer and Nicolson, 1972) was further enriched by the notion of lipid rafts with the discovery of heterogeneous membrane patches enriched in sphingolipids and sterols floating in the bilayer (Simons and Ikonen, 1997). Specific combinations of cellular environments, lipid classes, fatty acid length and saturation, and modes of membrane-protein association create a wide repertoire of membrane inhomogeneities. They mostly fall in what is called the mesoscale domain (larger than a nm but smaller than a μm) and have been classified based on their size and structure (Kusumi *et al.*, 2011). The largest domains, the 'membrane compartments', are proposed to be the result of partitioning of the entire plasma membrane by interactions between the actin-based membrane skeleton (fence) and transmembrane (TM) proteins anchored to the membrane skeleton fence (pickets). Smaller domains arise by the cooperative interactions between lipids and/or proteins with higher affinities for each other, that give rise to highly dynamic, steady-state lipid rafts, protein oligomers and other structures (Figure 2.1). From generalized membrane polarity, as in the case of the luminal and basolateral plasma membranes of epithelial cells, to caveolae and the spatially resolved

sites of endocytosis and exocytosis, or the sites of septation in fungal cells, there is wide variety in the scale and stability of these domains (Foderaro, Douglas and Konopka, 2017).

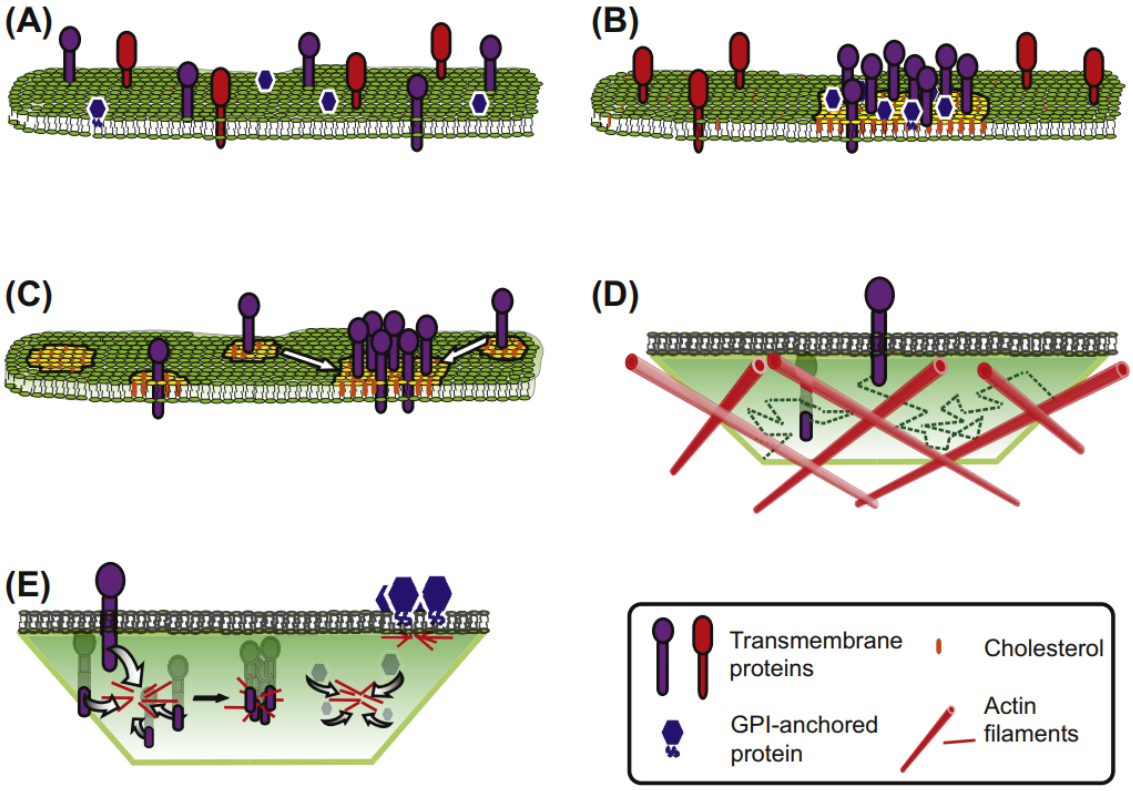

Figure 2.1 Evolution of plasma membrane organization models

(A) Fluid mosaic model. Transmembrane and membrane-associated proteins are distributed randomly through a homogenous phospholipid bilayer. (B) Lipid raft model. Sphingolipid and cholesterol selfassembled patches. Proteins which have an affinity for these patches preferentially populate these compartments. (C) Lipid shell model. Some proteins are surrounded by selfassembled cholesterol and sphingolipid complexes which form a "lipid shell" around it. These "lipid shells" have an affinity for, and can coalesce with, larger lipid domains. (D) Picket Fence model. Transmembrane protein diffusion is restricted by actin filaments (the "fence") which are anchored to other membrane-associated proteins ("pickets", not shown) and run parallel to the cytoplasmic leaflet of the membrane. (E) Active composite model. A very recent model according to which dynamic short actomyosin complexes adjacent to the cytoplasmic membrane leaflet attract specific transmembrane proteins and GPI-anchored proteins to each other. These complexes are arranged in "asters" and result in protein nanoclustering in the PM. (Curthoys *et al.*, 2015)

Despite the obvious biomedical interest for research on mammalian cells, the budding yeast *Saccharomyces cerevisiae* remains an ideal platform for the study of membrane organization and compartmentalization. In addition to the classical lipid rafts, small dynamic patches, that are enriched in sphingolipids and cholesterol (ergosterol in fungi)

and other domains that have been reported for both mammalian and fungal cells (Mollinedo, 2012), fungi and some algae also possess larger, more stable and static domains termed EMC/eisosomes. Their analogy to caveolae has been suggested based on striking similarities in structural, molecular and ontological characteristics (See Moreira *et al.*, 2012), but their stability and size allow for easier observation and manipulation. Several new, partially overlapping and coexisting microdomains were identified in yeast in a wide scale study of the plasma membrane proteome (Spira *et al.*, 2012). Along with the immense variety of lipid species present in even simple organisms like yeast (Ejsing *et al.*, 2009; Guan *et al.*, 2010), that are only now being better appreciated with lipidomic techniques gaining ground (Wenk, 2010; Han, Yang and Gross, 2012), the emerging view regarding biological membranes and the plasma membrane in particular, is that of a self-organizing, through both individual and aggregate interactions, network of multiple compartments, or 'patchwork membrane' (Müller, Wedlich-Söldner and Spira, 2012).

Overall, even though the significance of the compartmentalization of PM components has been appreciated recently, the diversity in underlying mechanisms and compartments, as well as the prevalence of these phenomena cannot yet be accurately predicted (Lingwood and Simons, 2009; Bagatolli *et al.*, 2010).

2.2. The EMC/eisosome structure

Furrow-like invaginations of the plasma membrane were probably first identified in yeast over 50 years ago (Moor and Mühlethaler, 1963). Much later, membrane patches with distinct protein composition were reported in yeast for the first time (Malínská *et al.*, 2003), although the link between the two structures remained elusive for another six years, until it was shown that they constitute the same subcellular structure (Strádalová *et al.*, 2009).

These invaginations, termed eisosomes because of their inward curvature, are approximately 200-400 nm long, 30 nm wide and 50 nm deep (Figure 2.2) (Moor and Mühlethaler, 1963; Strádalová *et al.*, 2009). Their number per cell varies based on cell size between 20 and 50 and they show a relatively constant density on the plasma membrane

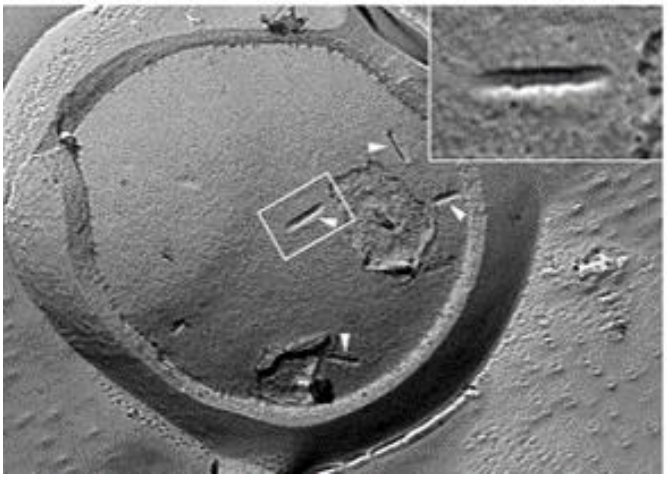

Figure 2.2 Eisosome invaginations are clearly visible in SEM images

Freeze fracture SEM image of a budding yeast cell showing the characteristic invaginations (white arrows) of eisosomes. (Strádalová *et al.*, 2009)

(Olivera-Couto *et al.*, 2015). They are composed of an intracellular protein coat made up from Pil1 (**P**hosphorylation **i**nhibited by **l**ong-chain bases) and Lsp1 (**L**ong-chain bases **s**timulate **p**hosphorylation), two paralogous BAR-domain (**B**in-**A**mphiphysin-**R**VS) proteins, that form dynamic homo- and heterooligomers that bind to and stabilize the characteristic membrane curvature by interactions with lipids (Walther *et al.*, 2006; Karotki *et al.*, 2011; Olivera-Couto *et al.*, 2011). Each invagination is calculated to be composed mainly of 2000-5000 copies of these two proteins (Walther *et al.*, 2006). Pil1 is regarded as the main eisosomal organizer, as null mutants lack eisosomes almost completely and possess a limited number of aberrant structures called 'eisosome remnants' composed solely by Lsp1 (Walther *et al.*, 2006; Grossmann *et al.*, 2007). While *PIL1* is a nonessential gene, null mutants exhibit several phenotypes including notably increased sensitivity to osmotic stress (Yoshikawa *et al.*, 2009) and decreased rate of endocytosis (Walther *et al.*, 2006). The crystal structure of Lsp1 has been determined for residues 36-267, showing that it dimerizes (Karotki *et al.*, 2011), as is probably the case for Pil1 as well, based on the high degree of sequence identity between them (Huh *et al.*, 2003). *PIL1* (and *LSP1*) expression levels oscillate during the cell cycle so that eisosomes are formed in the daughter cell early in bud development from Pil1 that is actively transported from the mother cell (Moreira *et al.*, 2008) and are then rendered immobile

and their number remains constant throughout the life cycle. Other proteins, like the BAR-domain Slm1/2 and the Pkh1/2 kinases (See below) may localize to eisosomes only transiently, or as part of the biogenesis of the organelle. One important example is Seg1 which drives the deposition of Pil1 in growing eisosomes in a process very similar to caveolar biogenesis and lack of which leads to fewer, deformed invaginations (Moreira *et al.*, 2012).

The corresponding membrane patches, hereafter called EMCs (**E**isosome-associated **M**embrane **C**ompartment) when referring exclusively to the membrane component, were originally termed MCCs (Membrane Compartment of Can1) in juxtaposition to the network-like MCP (Membrane Compartment of Pma1) as the two proteins were thought to be located in mutually exclusive compartments (Malínská *et al.*, 2003). Along with the MCT (Membrane Compartment of TORC2) which is postulated to specifically house the Target of Rapamycin Complex 2 (TORC2) (Berchtold and Walther, 2009), these are the first discovered and best characterized compartments in the plasma membrane of yeast. Pma1, the main H^+-ATPase, is the most abundant integral plasma membrane protein and the main determinant of plasma membrane potential and possibly cytosolic pH (Serrano, Kiellandbrandt and Fink, 1986). It is excluded from the EMC, probably because of steric exclusion of the large oligomeric complexes it forms from the subcortical protein core (Bianchi *et al.*, 2018). Proteins concentrated in the EMC notably include nutrient transporters such as Can1, Fur4, Tat2, Mup1 and Lyp1 (Grossmann *et al.*, 2007; Malínská *et al.*, 2004, 2003; Spira *et al.*, 2012; Unpublished lab observations), and tetraspan proteins like Sur7 and Nce102. Their exact mode and possible mechanism of concentration varies, as for example Sur7 is found solely in EMCs (Walther *et al.*, 2006; Fröhlich *et al.*, 2009), while Nce102 and nutrient transporters dynamically change localization as discussed below (Grossmann *et al.*, 2007, 2008; Fröhlich *et al.*, 2009). Sur7 (**Su**ppressor of **R**vs167 mutation) is an integral membrane protein found exclusively in the EMC whose role remains unclear, although null mutants have abnormal sphingolipid metabolism (Young *et al.*, 2002). Nce102 is a MARVEL-domain protein, is required for the

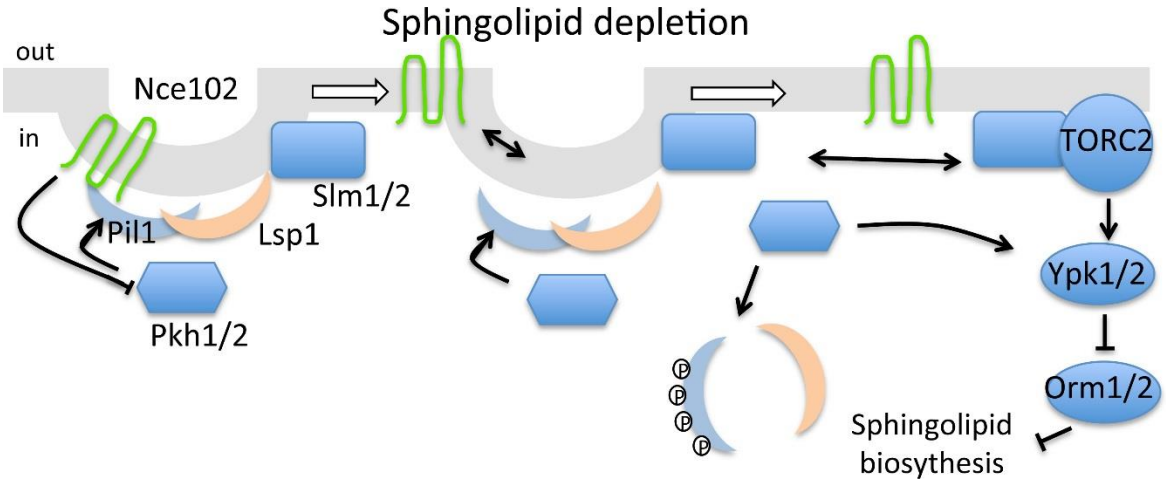

Figure 2.3 Sphingolipid sensing and EMC/eisosome disassembly

The figure illustrates the regulatory pathway described in the text, highlighting the proposed role of Nce102 as a sphingolipid sensor. (Gournas *et al.*, 2018, SI)

organization of eisosomes and is proposed to be involved in sphingolipid sensing (Fröhlich *et al.*, 2009; Berchtold *et al.*, 2012). It has been identified as a repressor of the Pkh1/2 kinases (Fröhlich *et al.*, 2009). In the SL-sensing pathway, upon depletion of SLs, Nce102 becomes homogenously distributed (Fröhlich *et al.*, 2009), alleviating its constitutive repression of the eisosome-residing Pkh1/2 kinases which can then phosphorylate Pil1 and Lsp1 in a specific pattern (Luo *et al.*, 2008), leading to disassembly of Pil1 and the eisosome protein core (Figure 2.3) (Walther *et al.*, 2007; Luo *et al.*, 2008), an effect also mimicked by the deletion of Nce102 as the Pkh kinases are derepressed (Fröhlich *et al.*, 2009). This correlates with a relocalization of the Slm1/2 proteins to the MCT to activate the Ypk1/2 kinases (Berchtold *et al.*, 2012). The TORC2-phosphorylated Ypk1 phosphoinhibits the Orm1/2 proteins (Roelants *et al.*, 2011), which are negative regulators of the serine:palmitoyl-coenzyme A transferase (SPT) (Breslow *et al.*, 2010) responsible for catalyzing the first step in *de novo* SL biosynthesis (Figure 2.4) (Nagiec *et al.*, 1994). The Pil1(4A) mutant used in this study is not phosphorylatable by the Pkh kinases, because of the substitution of the four target serines to alanines. Cells expressing

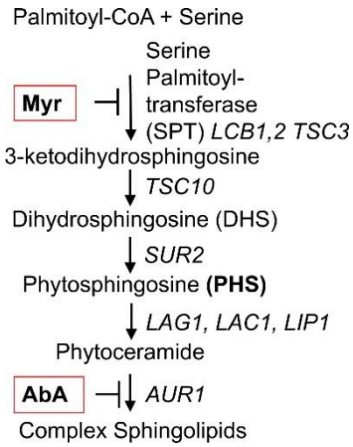

Figure 2.4 The sphingolipid biosynthesis pathway of budding yeast

Intermediate metabolites and genes involved are shown. The specific inhibitor of SPT, myriocin, as well as another inhibitor of the pathway, aureobasidin A, are highlighted (Red squares). PHS can be supplemented externally to rescue the effect of myriocin. (Gournas *et al.*, 2018)

this mutant retain their EMC/eisosomes even upon complex SL biosynthesis inhibition or deletion of *NCE102* (Walther *et al.*, 2007; Fröhlich *et al.*, 2009).

It has been previously shown by filipin staining that EMCs concentrate ergosterol (Grossmann *et al.*, 2007). Ergosterol is known to preferentially interact with sphingolipids and given the data above it has been suggested that EMCs concentrate these lipids as well (Fröhlich *et al.*, 2009), possibly leading to the creation of a lipid-ordered phase with slower diffusion rate. Sterols and phosphatidylethanolamine (PE) are two classes of lipids associated with membrane deformation and curvature, and interestingly, PE is required for the correct targeting of Can1 to the plasma membrane (Opekarová, Robl and Tanner, 2002).

Overall, the physiological role of EMC/eisosomes is not yet completely clear. Their implication in sphingolipid sensing and metabolism was summarized above. They were initially identified as static sites of endocytosis (Walther *et al.*, 2006), although later reports have been more cautious (Grossmann *et al.*, 2008). More recently they have been shown to not colocalize with sites of clathrin-mediated endocytosis, both in yeast (Brach, Specht and Kaksonen, 2011) and in *Aspergillus nidulans,* where deletion of both *PILA* and *PILB* has additionally been shown to not affect the rate of fluid-phase endocytosis or the ammonium-induced endocytosis of amino acid transporters (Vangelatos *et al.*, 2009;

Athanasopoulos *et al.*, 2013). In yeast, lack of EMC/eisosomes does result in a lower rate of endocytosis, but this is probably because of the greater proximity of cortical ER to the PM, that hinders the formation of endocytic sites (Strádalová *et al.*, 2012).

2.3. Can1 Structure-Function, Regulation and Relevant Permeases

Can1 is an arginine-H+ symporter that functions as the main Arg permease of *Saccharomyces cerevisiae*. It was named after genetic experiments associated the locus with sensitivity to canavanine (Grenson *et al.*, 1966), an arginine analogue that is toxic to yeast and many other organisms. Along with most fungal amino acid transporters, it belongs to the **a**mino-acid-**p**olyamine-organo**c**ation (APC) superfamily. A cluster of closely related fungus-specific permeases forms the **y**east **a**mino-acid **t**ransporter (YAT) family (Transporter Classification TC: 2.A.3.10) that includes both broad- and high-specificity members. An important, but distant, member of this family is the external amino-acid sensor Ssy1, which has lost transport activity and now exerts transcriptional control over other transporters (Didion *et al.*, 1998; Iraqui *et al.*, 1999; Klasson, Fink and Ljungdahl, 1999). Accumulating evidence also point to a signaling role for some member, as for example for Gap1, the general amino-acid permease of *S. cerevisiae* (Donaton *et al.*, 2003).

APC transporters adopt the LeuT or 5+5 fold with two, intertwined, V-shaped clusters of 5 **t**rans**m**embrane **d**omains (TMDs) that exhibit two-fold pseudosymmetry around an axis perpendicular to the membrane plane. The substrate-binding site is located in a hydrophilic cleft that is formed in the space between these TMDs. All members of the YAT family have 12 TMDs, as is common for the superfamily, with TMDs 1-5 and 6-10 serving as the aforementioned groups. The length of the TMDs remains approximately stable across members with most of the variability limited to the N- and C-terminal tails and inter-TMD loops. As no YAT structure has yet been experimentally determined, insights into the structure-function relationships of these transporters have come from induced-fit modelling on bacterial homologues, notably AdiC, the Arg permease of *E. coli*, often with impressive results. From a molecular mechanics perspective, transporters can be

crudely thought of as transitioning from an outward-facing (OF) to an inward facing (IF) conformation through a series of intermediates, a process driven by successive interactions with the substrate as it is channeled from the periplasm to the cytoplasm (Figure 2.5). This alternating-access transport model (Jardetzky, 1966) was later extended by the discovery that residues outside the binding pocket also confer substrate selectivity, functioning as a series of gates (Diallinas, 2008), as do inter-TMD loops in some APCs (Yamashita *et al.*, 2005; Krishnamurthy and Gouaux, 2012). Interestingly, this may also be the case for Can1 since mutations in these regions have been reported to show altered specificity (Regenberg and Kielland-Brandt, 2001).

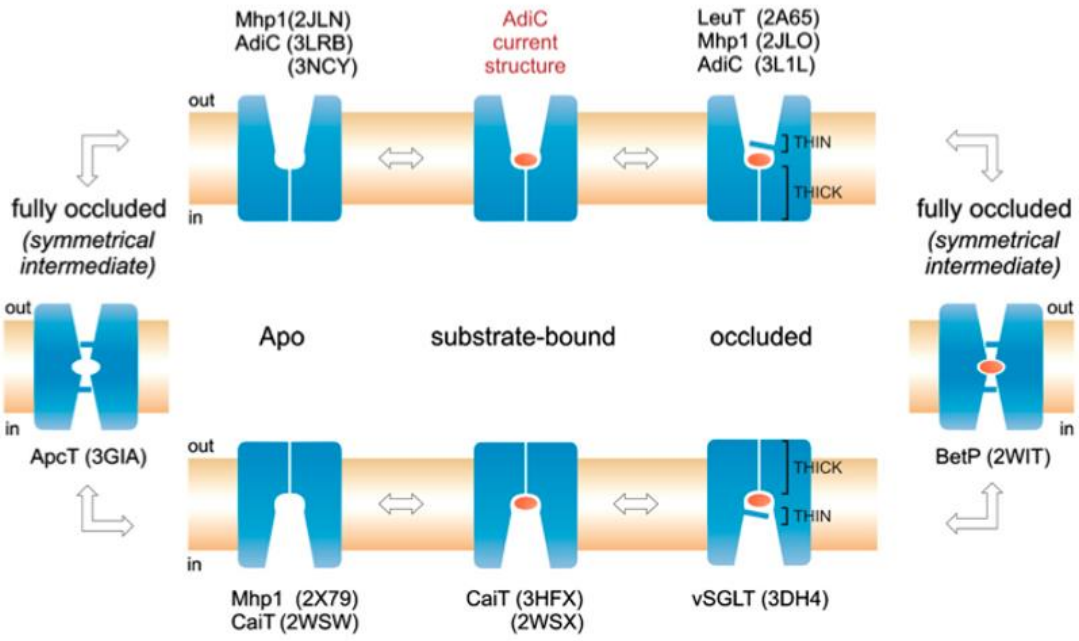

Figure 2.5 Schematic representation of transport cycle states

Experimentally determined structures of APC superfamily members show the multitude of intermediate states a transporter occupies during the transport cycle. Substrate is seen in red. In the occluded states, the gates can be seen as bars concealing the substrate binding site. (Kowalczyk *et al.*, 2011)

Substrate recognition in YATs involves residues from several TMDs. The α-amino and α-carboxyl groups of the amino acid interact via hydrogen bonds with two motifs found on TMD 6 and 1 respectively (Ghaddar, Krammer, *et al.*, 2014; Gournas *et al.*, 2015) (Figure 2.6), which are also present in AdiC (Gao *et al.*, 2010). Residues from TMDs 3, 6, 8 and 10

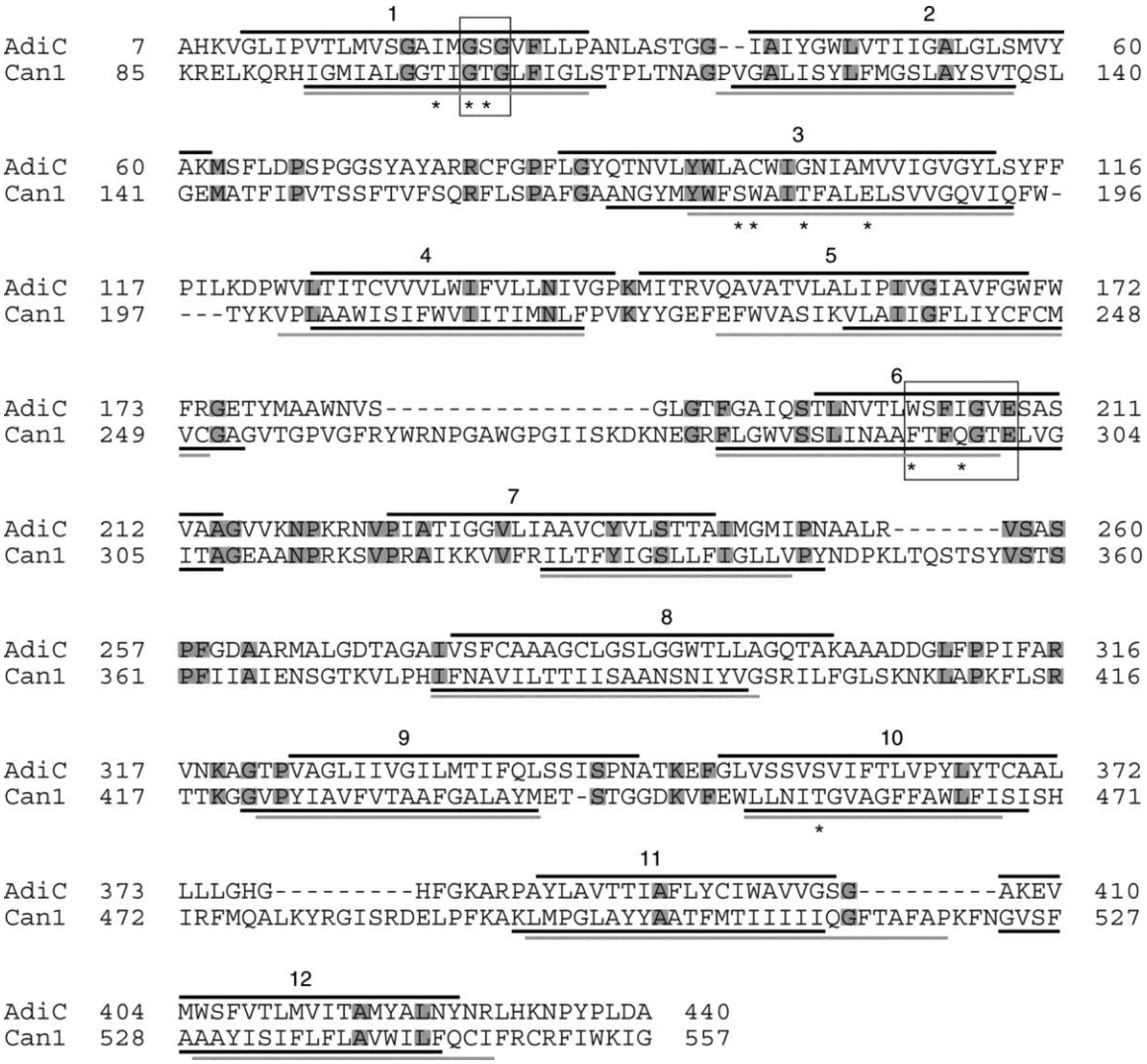

Figure 2.6 Sequence alignments of Can1 with AdiC

The alignment highlights important conserved residues that interact with the substrate (asterisks). Predicted TMDs for AdiC based on its crystal structure are shown as black lines above the AdiC sequence. Predicted TMDs on the Can1 sequence are shown as solid lines below the Can1 sequence. The two motifs mentioned in the text that interact with the α-carboxyl and α-amino groups are framed. Conserved residues in AdiC and Can1 are boxed in gray. (Ghaddar, Krammer *et al.*, 2014)

have been implicated in interactions with the side chains, but these are not well conserved as they should co-vary with transport specificities. Comparison of Can1 with Lyp1 and AdiC have revealed interesting features. Lyp1 is a close relative of Can1 and the main lysine permease of *S. cerevisiae*. They differ in their substrate-binding pockets in only two residues, Ser^{176} and Thr^{456} of Can1, corresponding to Asn^{193} and Ser^{478} of Lyp1. Substituting both residues in Can1 for their counterparts of Lyp1, results in a transporter with almost identical kinetic characteristics as the latter. Both residues are predicted to interact via hydrogen bonds with the substrates; the S176N mutation on its own results in a totally inactive mutant, probably due to steric hindrances of the larger side chain either with other residues or the substrate in the OF state (Gournas *et al.*, 2017), while the T456S mutation, which by itself slightly increases the Vmax for both substrates, is believed to influence function in a different manner, by alleviating restrictions on conformational changes that the transporter undergoes when transitioning from the OF to the IF state. In Can1, several other residues, notably Thr^{180}, are predicted to form hydrogen bonds with the substrate, which is sandwiched between the two aromatic rings of Trp^{177} and Phe^{295}. Similar to previously mentioned mutations, the inactive Can1(T180R) form used in this study has lost the capacity to bind arginine due to steric hindrances (Ghaddar, Krammer, *et al.*, 2014). One striking insight from comparisons between YATs and AdiC, comes from closer inspection of Can1 residue Glu^{184} which corresponds to Met^{104} of AdiC. *In silico* analysis predicted a correlation of Glu^{184} protonation state with the orientation of substrate side chains in the binding pocket of Can1. Given the fact that AdiC is not a proton antiporter like YATs, suggests an interesting mechanism where the protonation state of this residue in Can1 is the coupling point with proton export, involving movements in both the transporter and the substrate. Thus, the inactive E184Q and E184A mutants could represent two states mimicking the protonated and deprotonated forms constitutively. On the basis of this, Can1(E184Q) was predicted to be blocked in an IF state (Ghaddar, Krammer, *et al.*, 2014).

The expression of many nutrient transporters with strict specificity, notably Can1, Fur4 and Tat2, is regulated by the presence of their substrate (Séron *et al.*, 1999; Kodama *et*

al., 2002). On the post-translational level, transporters are downregulated by their substrate in several ways via the endocytic pathway (Ghaddar, Merhi, *et al.*, 2014). The initial step is mediated by the Rsp5/Nedd4 ubiquitin ligase, an E3 HECT enzyme (Hein *et al.*, 1995). Rsp5 transfers ubiquitin to Lys residues of target proteins. An adaptor protein is needed for recognition of most membrane proteins as they lack the classical PPxY target motifs. For transporters this is mediated by a family known as the α-arrestins composed of 14 members in yeast, that exhibit target-protein and stimulus specificity. Can1 substrate-induced ubiquitination, for example, depends on Art1 and residually on the Bul1/2 adaptors, but the latter are neither sufficient nor necessary to promote vacuolar sorting of the transporter (Gournas *et al.*, 2017). Intracellular levels of amino acids are known to activate TORC1, which notably promotes the internalization of Gap1 through inhibition of Npr1, a negative regulator of many arrestins (Merhi and André, 2012; Ghaddar, Merhi, *et al.*, 2014). Can1, however, is not subject to the same mode of regulation. It was recently shown that a conformation shift to an IF state is additionally required to expose the binding site of Art1 (Art1BS) in its N-terminal tail, as part of its transport cycle (Figure 2.7). This exposure is dependent on an intact tripeptide close to

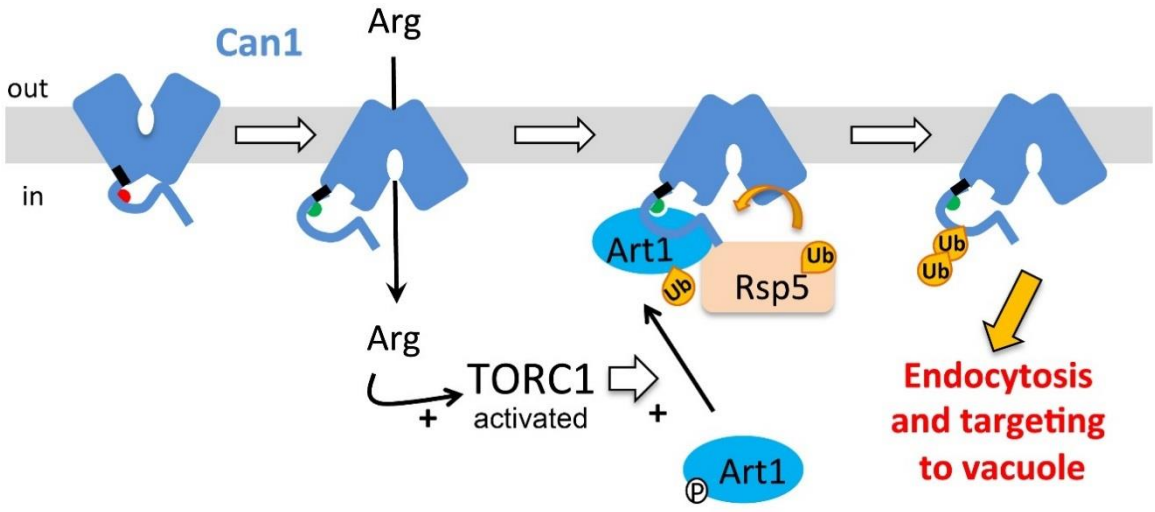

Figure 2.7 Steps in the substrate-induced ubiquitination and endocytosis of Can1

In its OF state the Art1BS is hidden. Upon transport of Arg Can1 transiently shifts to an IF state and the Art1BS is exposed. Intracellular Arg leads to the activation of Art1 and recruitment of the Rsp5 Ub-ligase to Can1, through the TORC1 pathway. Can1 is ubiquitinated and sorted for vacuolar degradation. (Gournas *et al.*, 2018)

TMD1, that seems to function as a molecular hinge, since mutants in this region constitutively expose the Art1BS. This masking mechanism, coupled to the activity of the transporter, has been proposed as an efficient mechanism of selective downregulation of permeases whose continued function could lead to toxicity. Mutation of either the Art1BS or the 7 target lysines, also located in the N-terminal tail, results in versions of Can1, the latter termed Can1(7KR), that remain stable at the plasma membrane in the presence of its substrate (Gournas *et al.*, 2017).

As mentioned above, Can1 has been shown to require PE for its correct targeting to the PM, while the same has been reported for ergosterol which also impacts its transport activity. A modulatory role for sphingolipids has been suggested as well, given that *NCE102*, a putative sphingolipid sensor also resides in and regulates EMCs (Loibl *et al.*, 2010). Sphingolipids are known to be required for correct folding of Gap1 prior to sorting to the plasma membrane (Lauwers, Grossmann and André, 2007). However, no specific lipid-interacting motif has been identified for a transporter to date.

In studies focusing on the partitioning of nutrient transporters in EMCs, the dynamic behavior of Can1 remains controversial. Although it is agreed that in the absence of its substrate, it localizes preferentially to EMCs, exit from the compartment upon addition of Arg (Grossmann *et al.*, 2008) has been directly disputed (Brach, Specht and Kaksonen, 2011).

2.4. Thesis Goals

The aim of this thesis was to uncover the mechanism and factors determining transporter enrichment in EMCs, a topic that remains unresolved, sometimes with conflicting reports. Eisosomes were initially identified as sites of vesicular trafficking (Walther *et al.*, 2006), a view that was later refuted in favor of a model arguing a role in protection from endocytosis (Grossmann *et al.*, 2008). However, this was also put into debate by directly measuring the rate of endocytosis of Can1 in cells lacking EMC/eisosomes (Brach, Specht and Kaksonen, 2011). So, despite the relatively well-established function of

EMC/eisosomes in sphingolipid homeostasis, the preferential association of nutrient permeases in the domain remains enigmatic.

Can1 was selected as a model given the knowledge and tools available to study it. By utilizing the mutants described above, its lateral plasma membrane segregation is effectively uncoupled from its ubiquitination status and endocytosis. Confocal-laser microscopy is used to measure quantitative variations in EMC enrichment and combined with data from kinetic and endocytosis-efficiency analyses and growth tests. Can1 mutants defective at specific steps of the transport cycle were analyzed in either *WT* or strains lacking EMC/eisosome components or under conditions of SL depletion by specific inhibitors of the biosynthetic pathway to elucidate the underlying mechanisms and potential physiological significance of the phenomenon.

3. Results

3.1. Validation of a quantification method for multi-channel laser confocal microscopy images

In order to study the mechanism and factors affecting the localization of Can1, a method was developed to reproducibly quantify the degree of enrichment of fluorescently tagged proteins in EMC/eisosomes in reference to an exclusive EMC or eisosomal marker protein, either Sur7 or Pil1. To calibrate the range of measurement, Sur7 and Gap1 were used as a maximum and minimum enrichment control, respectively, alongside Can1 (Figure 3.1).

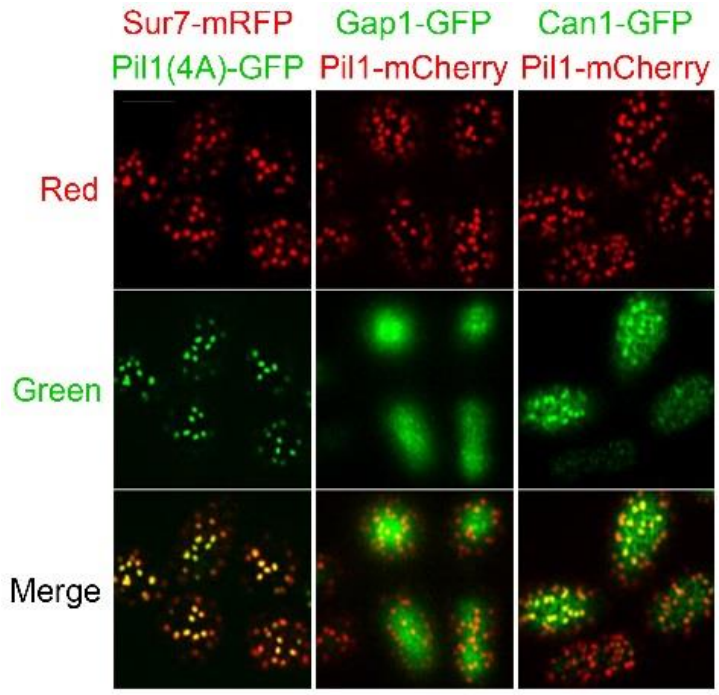

Figure 3.1 EMC-enrichment controls

Cells expressing GFP-, mRFP-, or mCherry-tagged eisosomal proteins and Can1-GFP or Gap1-GFP were observed by confocal microscopy coupled to Airyscan detection. Surface sections were acquired for quantifications and middle sections for assessment of Pil1 dissociation and/or transporter internalization.

Custom-written ImageJ macros to automate cell measurements, initially developed by Dr. Twyffels based around two approaches were further developed: a pixel-by-pixel analysis measuring the Pearson's correlation coefficient, R, for the two proteins, and an object-based approach, using the channel of the marker protein to identify EMC/eisosomes and

then measure the fluorescence intensity ratio of the protein under analysis in EMC over the rest of the plasma membrane surface. While both approaches capture differences in the degree of enrichment (Figure 3.2 Left), the object-based analysis was finally preferred, because the change in values linearly represents a times-change in enrichment, in contrast with the more complicated interpretation of the Pearson's coefficient that only conveys the goodness-of-fit to a linear relationship. It is worth noting, that Pearson's correlation values also lead to very reproducible analyses (Figure 3.2 Right).

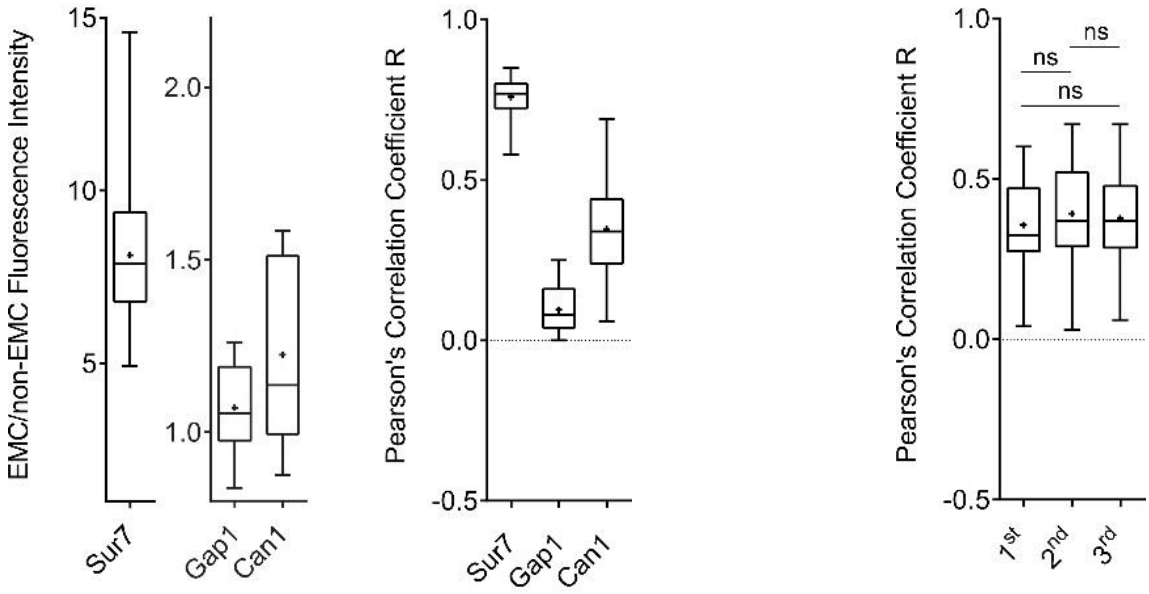

Figure 3.2 Quantification of EMC-enrichment controls

(Left) EMC-enrichment of Sur7-mRFP, Gap1-GFP and Can1-GFP quantified using both approaches (n = 15-30 cells). The horizontal midline and the cross represent the median and average values, respectively. Each box is bounded by the upper and lower quartiles; the whiskers denote the maximal and minimal ratios. (Right) The reproducibility of the Pearson's correlation coefficient is highlighted by three independent biological replications of Can1-GFP EMC-enrichment quantifications. ns, nonsignificant, $P > 0.05$.

Representative steps in the object-based analysis pipeline are shown (Figure 3.3). This approach is also less influenced by signal fluctuations within each compartment or from optical effects, that are irrelevant to the analysis and which would lead to an erroneous estimation of EMC-enrichment based on the Pearson's coefficient. An important limitation, however, is that it depends on a higher signal to noise ratio for the accurate recognition of EMCs.

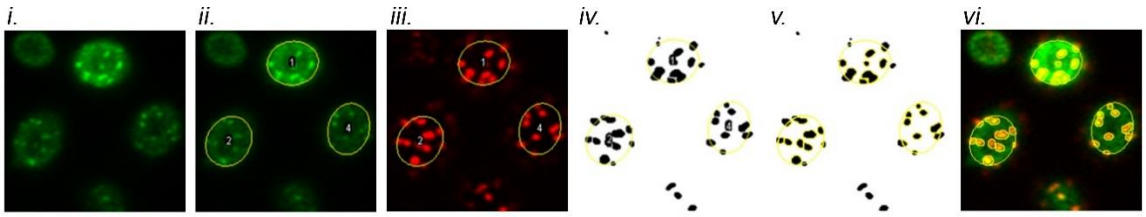

Figure 3.3 Representative steps of the custom written EMC-detection and analysis macro

i. Channel of the protein to be analyzed. ii. Cell outlines were drawn manually using the ellipse tool based on the analyzed protein signal. iii. The EMC/eisosome marker protein channel was despeckled using a 3×3 median filter and then thresholded using default ImageJ parameters to create a mask of EMCs. iv. The resulting mask was watershed with default parameters to separate neighboring EMCs. v. Individual EMCs were identified based on this processing and the fluorescence intensity and area was measured both for the entire cells and the EMC occupied fraction. vi. Resulting overlay

3.2. Can1 loses enrichment upon transport of its substrate in a ubiquitination-independent manner

Previous reports on the plasma-membrane localization of Can1 in the presence of its substrate have been conflicting. An early time-course experiment indicated no change in enrichment even 400 min after substrate addition, in contrast with Tat2 that became homogenous within 90 s (Brach, Specht and Kaksonen, 2011). Later observations however, pointed to a similar behavior for Can1 as well, even in conditions where Can1 ubiquitination is inhibited (Gournas *et al.*, 2017, uncommented; Unpublished lab observations). Preliminary experiments showed a patchy distribution corresponding to EMC/eisosomes for Can1 but not Gap1 in the absence of their respective substrates (See Figure 3.1), in accordance with past literature (Malínská *et al.*, 2003, 2004). Upon addition of arginine, Can1 progressively loses its enrichment, with a very fast onset (Unpublished lab observations), comparable with that reported for Tat2. This effect is even more pronounced at later timepoints, where Can1 is almost homogenously distributed. This is evident in conditions under which the ubiquitination and substrate-induced endocytosis of Can1 have been inhibited by using the fully functional non-ubuiquinatable Can1(7KR) mutant, or by deleting the genes for the arrestins responsible, *ART1, BUL1* and *BUL2*, in order to prevent internalization that would hamper the quantification of PM protein

(Figure 3.4). This result also highlights the fact that exit from EMCs is a phenomenon independent from Can1 ubiquitination.

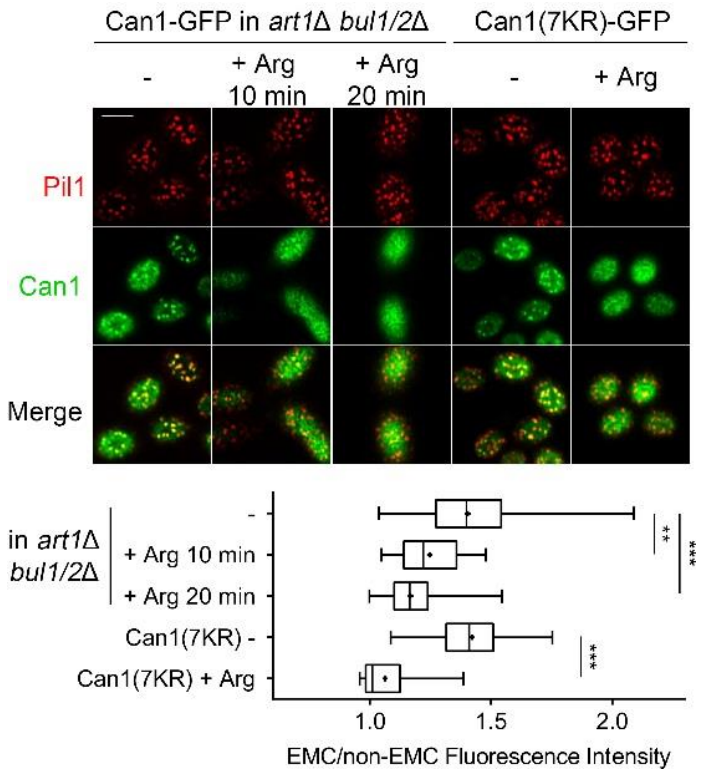

Figure 3.4 Can1 exits EMCs in a substrate dependent and ubiquitination independent manner

Surface section confocal images of an *art1*Δ *bul1/2*Δ and a *WT* (*PIL1-mCherry gap1*Δ *can1*Δ) expressing *pGAL1* driven Can1-GFP or Can1(7KR)-GFP. Cells were grown in Gal Pro medium and switched to Glu 1.5 h before observation. Quantifications (n = 15-35 cells) are as in Fig. 2.2. ***, P < 0.001; **, 0.001 < P < 0.01. (Scale bar: 3 µm.)

Since Can1 is the sole arginine transporter expressed in this setup, these results open up two possibilities: Firstly, that exit from EMCs is caused directly by transport of substrate and, secondly, that it is the indirect result of sensing intracellular amino acids. In support of the first hypothesis, when an inactive mutant such as Can1(T180R) is used, no change in its enrichment is observed, even when a non-tagged, active form of Can1 is co-expressed (Gournas *et al.*, 2018). In agreement with this scenario, the lysine-specific Can1(S176N,T456S) mutant does not respond to addition of arginine (Figure 3.5).

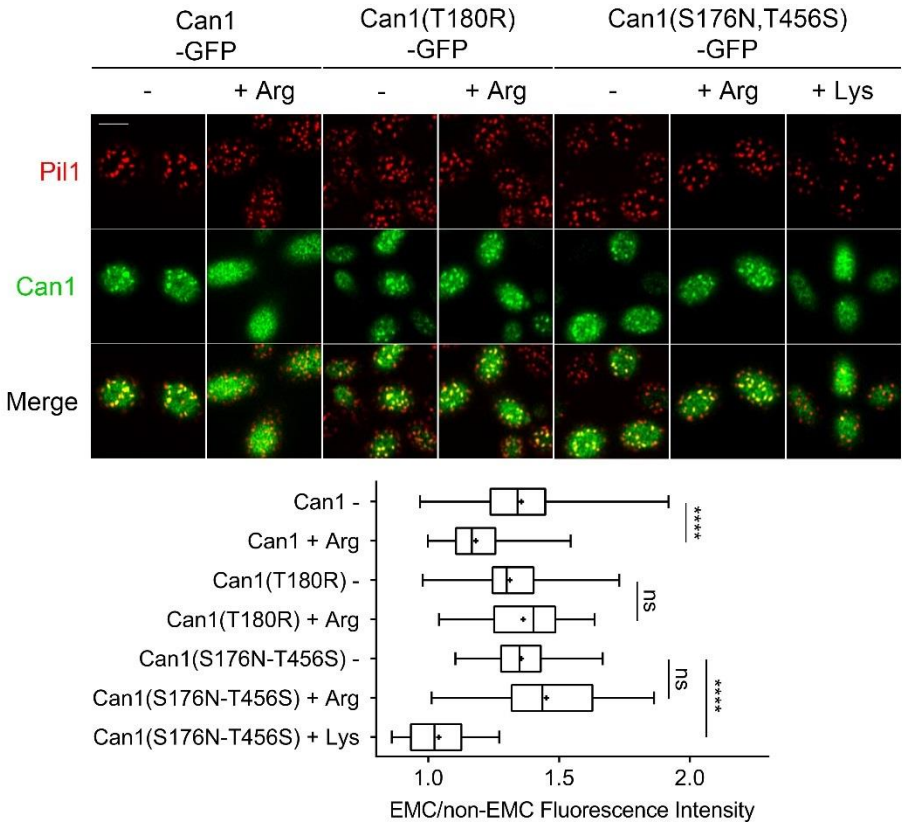

Figure 3.58 Activity dependent exit from EMCs

Surface section confocal images of a *WT* (*gap1*Δ *can1*Δ *PIL1-mCherry*) strain expressing *pGAL1* driven Can1-GFP, Can1(T180R)-GFP, or Can1(S176N,T456S)-GFP. Conditions and quantifications (n = 20-40 cells) are as in Fig. 2.4. ****, P < 0.0001; ns, nonsignificant, P > 0.05. (Scale bar: 3 µm.)

3.3. Conformation driven segregation of Can1 in EMCs

The data above point to an intrinsic aspect of Can1 itself modulating its PM distribution. This could be attributed to a signaling capacity of the transporter, or another specific interaction, or possibly to a conformational change. Given that exit from EMCs seems to coincide with transition from an OF to an IF conformation as part of the transport cycle, it appears likely that the two events are linked.

The Can1(S176N) mutant, which is unable to transition to the IF due to steric hindrances, is not affected by arginine and remains enriched in EMCs (Figure 3.6 Left). Strikingly, Can1(E184Q), predicted to be blocked in the IF state, constitutively shows no EMC enrichment. This effect is not observed for Can1(E184A), which supports the notion that the different protonation states of E184, as mimicked by the two substitutions, result in

different conformations for the transporter that in turn determine its localization (Figure 3.6 Right). Notably, all these versions of Can1 are completely inactive (Ghaddar, Krammer, *et al.*, 2014).

As all these mutations reside in the substrate-binding site and therefore do not directly alter the surface of the protein, the conformational state seems to determine whether Can1 is preferentially localized in EMCs. It also highlights the importance of the Glu^{184} residue in modulating localization through its transitioning between the protonated and unprotonated form (See Introduction).

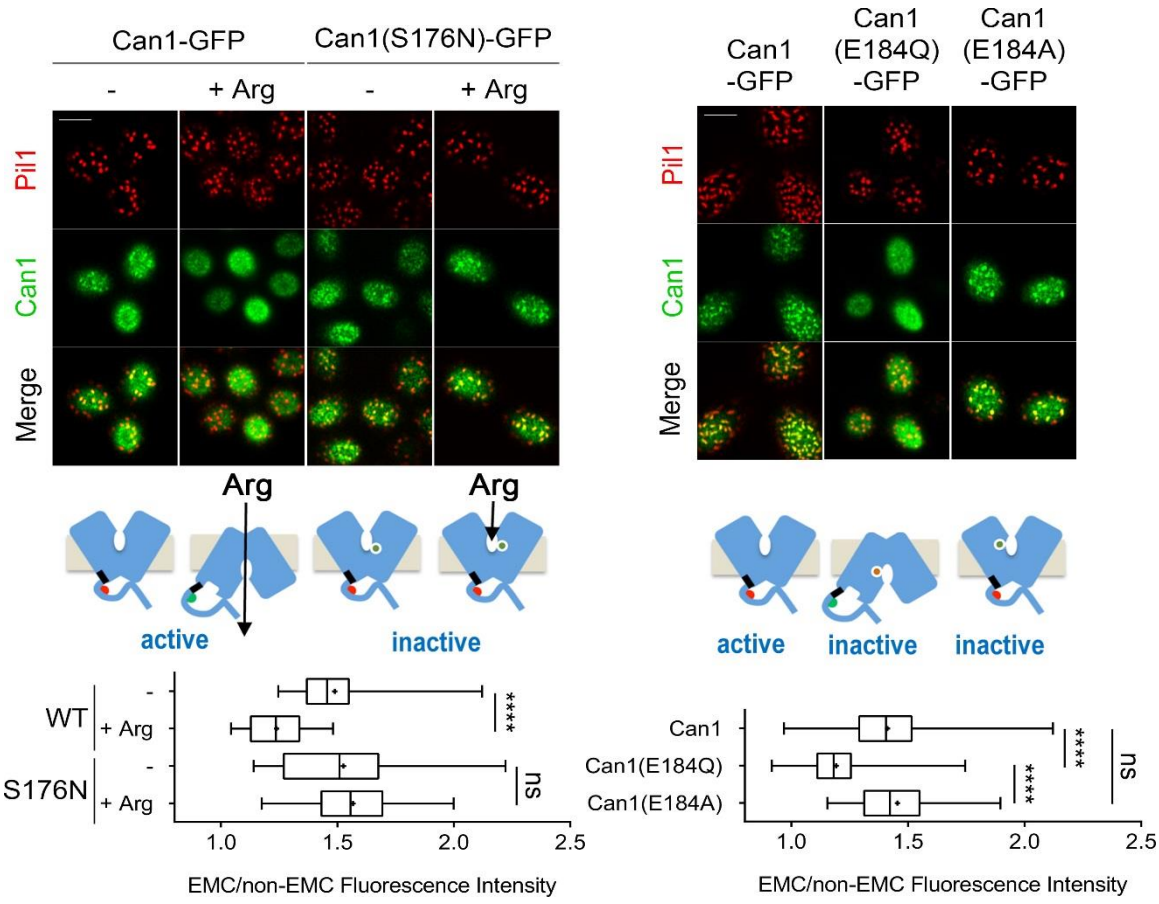

Figure 3.6 Conformation dependent partitioning of Can1 in the plasma membrane

Section confocal microscopy images and quantification of (Left) an *art1*Δ *bul1/2*Δ (*gap1*Δ *can1*Δ *PIL1-mCherry*) strain expressing Can1-GFP or Can1(S176N)-GFP and (Right) a *WT* (*gap1*Δ *can1*Δ *PIL1-mCherry*) strain expressing Can1-GFP, Can1(E184Q)-GFP, or Can1(E184A)-GFP. Conditions and quantifications (n = 25-40 cells) are as in Fig. 2.4. The cartoons summarize previous knowledge (25, 32). The E184Q substitution stabilizes the transporter in an IF state, permanently exposing the Art1BS even in the absence of substrate. ****, $P < 0.0001$; ns, nonsignificant, $P > 0.05$. (Scale bar: 3 µm.)

3.4. Complex sphingolipid depletion also causes loss of enrichment

The mechanistic basis of EMC enrichment was studied next. Given the evidence indicating the concentration of sphingolipids in EMCs (Grossmann *et al.*, 2007, 2008; Fröhlich *et al.*, 2009; Berchtold *et al.*, 2012), it was reasonable to hypothesize they could play a role in the localization patterns of resident proteins.

To test this, a specific sphingolipid biosynthesis inhibitor, myriocin, was used to deplete cells of complex sphingolipids. Myriocin inhibits the SPT and its phenotype can be rescued by supplying the product of this enzyme, phytosphingosine, externally. Since Pil1 is phosphorylated and dissociates from eisosomes upon sphingolipid depletion (See Introduction), the Pil1(4A) mutant was used which has been shown to be resistant to this

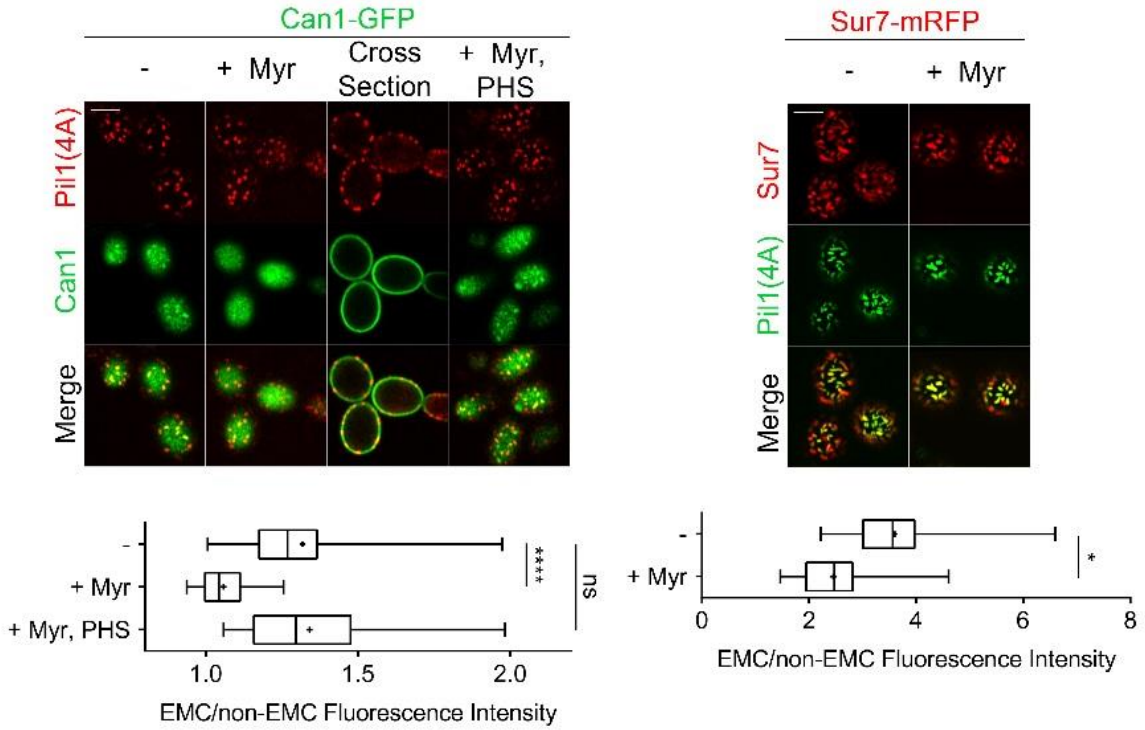

Figure 3.7 Intact sphingolipid biosynthesis is required for Can1 EMC enrichment

Surface and middle section confocal microscopy images of (Left) a *PIL1(4A)-mRFPmars gap1*Δ *can1*Δ strain expressing Can1-GFP and (Right) *PIL1(4A)-GFP gap1*Δ *can1*Δ strain expressing Sur7-mRFP. Wild type Pil1 is not expressed in either strain. Cells were grown in Gal Pro medium. Glu was added for 1.5 h and then 10 µM Myr or 10 µM Myr + 10 µM PHS was added for 1.5 h. Quantifications (n = 30-50 cells) are as in Fig. 2.4 ****, $P < 0.0001$; *$P < 0.05$; ns, nonsignificant, $P > 0.05$. (Scale bar: 3 µm.)

type of regulation (Walther *et al.*, 2007; Fröhlich *et al.*, 2009). Cells treated with myriocin show almost total loss of Can1 EMC enrichment, a phenotype that is rescued when phytosphingosine is added (Figure 3.7 Left). Sur7 remains almost completely unaffected upon this treatment, indicating that at least in these conditions, EMC/eisosomes remain intact (Figure 3.7 Right). This suggests that sphingolipids, either directly or indirectly, are required for the preferential partitioning of Can1 in EMCs. Upon depletion, the distribution of Can1 becomes homogenous.

Another line of evidence for the concentration of sphingolipids in EMCs, comes from the fact that the membrane extractability of Can1 using the Triton X-100 detergent decreases upon addition of arginine (Grossmann *et al.*, 2008), or when the Can1(E184Q) mutant is used instead (Figure 3.8). Since detergent resistance of membrane proteins is usually associated with residency in sterol- and sphingolipid-enriched membranes (Schröder, London and Brown, 1994; Hanada *et al.*, 1995), these results support both the hypotheses that Can1 exit from EMCs occurs upon a shift to an IF conformation, which is mimicked by the E184Q mutation, and also that EMCs are enriched in sphingolipid species.

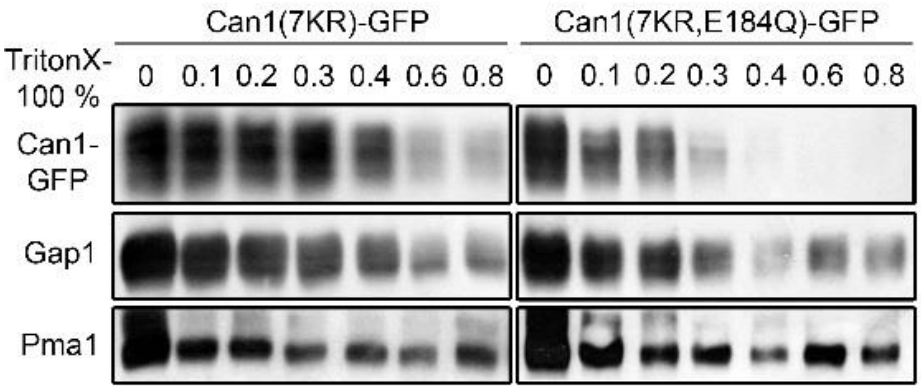

Figure 3.8 Detergent resistance of Can1(7KR) and Can1(7KR,E184Q)

In a *can1*Δ strain either Can1(7KR)-GFP or Can1(7KR,E184Q)-GFP was expressed under the *GAL1* promoter. Cells were grown in Gal Pro medium, and Glu was added for 1.5 h. 30-µg aliquots of membrane-enriched protein extracts were treated with increasing concentrations of Triton X-100. Following centrifugation and washing, the detergent-resistant insoluble pellet was resuspended in sample buffer and immunoblotted.

3.5. Can1 activity is unaffected by the absence of EMCs

It has previously been suggested that transporter EMC-residency plays a role in regulating their transport activity by providing a suitable lipidic environment (Spira *et al.*, 2012). Since no conclusive physiological role has been demonstrated for the EMC enrichment of nutrient transporters, this was the next topic of focus. Preliminary growth tests for canavanine resistance showed no effect in strains lacking *PIL1* or *SUR7* (Figure 3.9), two important EMC/eisosomal proteins.

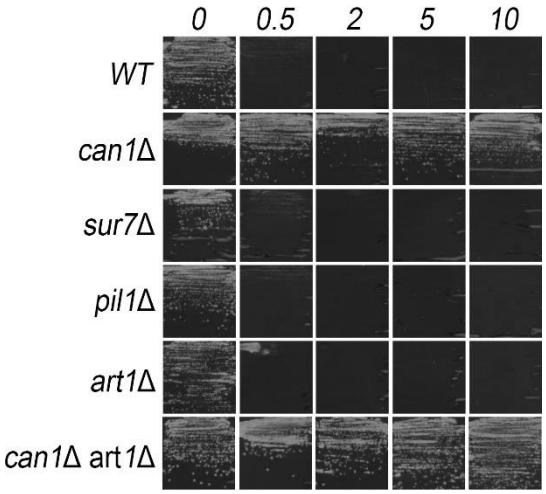

Figure 3.9 Canavanine resistance of strains lacking EMC/eisosome components, Can1 and/or Art1

Growth tests of a *WT*, a *can1*Δ, a *sur7*Δ, a *pil1*Δ, a *pGAL::CAN1 art1*Δ strain expressing an inactive form of Can1 and a *can1*Δ *art1*Δ (*gap1*Δ) strain on minimal synthetic medium containing increasing concentrations of canavanine (in µg/ml). Growth was observed after incubation for 48 h at 29°C.

The kinetic characteristics of Can1, as measured by substrate uptake assays of radiolabeled arginine, also showed no change in the apparent K_m between a *WT* and a *pil1*Δ strain (Figure 3.10 a). Interestingly, a decrease of around 20% was observed in the V_{max}. This could be attributed either to Can1 being less functional, or, alternatively, to a decrease in the quantity of Can1 at the plasma membrane, as the V_{max} directly correlates with the protein levels of the transporter. Quantifications of Western blotting analysis, normalized over the amount of Pgk1, a common reference protein because of its stable expression levels, has shown that less Can1 is present at the plasma membrane of *pil1*Δ strains (Figure 3.10 b). As these strains lack EMCs, which have previously been calculated

to house about 28% of the total Can1 (Brach, Specht and Kaksonen, 2011), these results show that less Can1 is present at the plasma membrane of *pil1*Δ cells. EMC/eisosomes have been calculated to comprise up to 20% of the cell surface (Brach, Specht and Kaksonen, 2011; Kabeche, Howard and Moseley, 2015) and because of their curvature they provide an extra 5-10% membrane surface area to act as a reservoir, to accommodate rapid cell expansion (Kabeche, Howard and Moseley, 2015). Thus, *pil1*Δ cells lacking invaginations have a lower surface-to-volume ratio, since the volume of these cells remains unchanged based on perimeter measurement (Table 3.1).

Table 3.1 Mean perimeters of WT and pil1Δ cells

The perimeter of cells of a WT and a pil1Δ strain were measured from wide-field epifluorescence microscopy images (n = 50)

	WT	*pil1*Δ	P-value of difference
Perimeter (µm)	13.75	13.46	0.9349, ns

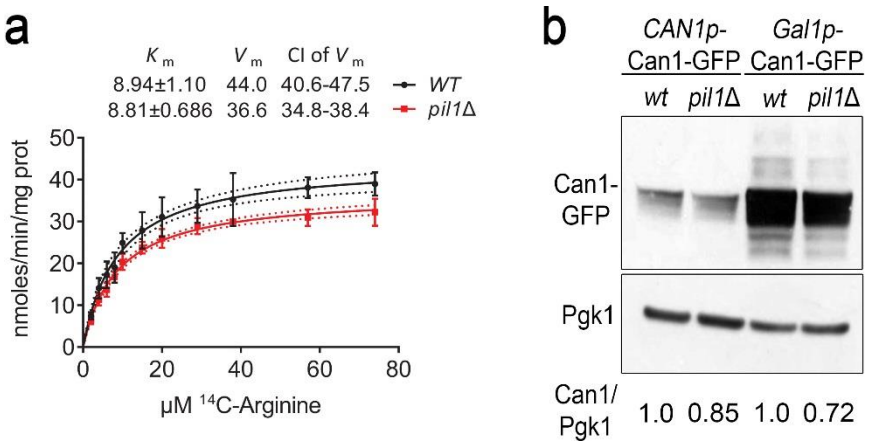

Figure 3.10 Lack of EMC/eisosomes only affects Can1 quantity and not its activity

(a) Concentration-dependent kinetics of [^{14}C]Arg uptake in a *WT* and a *pil1*Δ (*gap1*Δ) strain. Error bars indicate the SD; n = 3. Curve fitting and calculation of the V_{max} and K_m values (in µmoles), 95% CI (dotted curves) and F-pvalues were carried out by Michaelis–Menten analysis. Values reported at 3 significant digits. F-pvalue of Vmax = 0.0003, F-pvalue of Km = 0.9245. (b) Western blotting of *gap1*Δ *can1*Δ and *gap1*Δ *can1*Δ *pil1*Δ cells expressing Can1-GFP from the native or *GAL1* promoter, grown in Glu Pro or Gal Pro medium, respectively. Glu was added to the latter for 1.5 h before cells were collected. Total protein extracts were immunoblotted with anti-GFP and anti-Pgk1. Quantifications shown below the blots are the ratios of Can1-GFP/Pgk1 intensities. Ratios in the *PIL1*$^+$ (*WT*) strain are set at 1. The heavier bands above Can1-GFP were not quantified, as they have been shown to correspond to ubiquitinated forms of Can1 (Gournas *et al.*, 2017).

The lower levels of Can1 in *pil1*Δ cells could indicate either a specific effect on EMC-resident proteins in cells lacking EMC/eisosomes or a generalized decrease in PM-protein levels due to loss of membrane surface area. In order to discriminate between the two scenarios, the transport activity of Gap1, a permease not preferentially segregating in EMCs. In line with the first scenario, the apparent V_{max} for the uptake of radiolabeled citrulline by the non EMC-enriched Gap1 is much more mildly affected in the *pil1*Δ strain (Figure 3.11). These results strongly indicate that in *pil1*Δ cells there is a specific decrease in the levels of EMC-resident proteins only. Interestingly, the apparent K_m of Gap1 in *pil1*Δ cells decreases significantly, a result for which no apparent explanation is currently available.

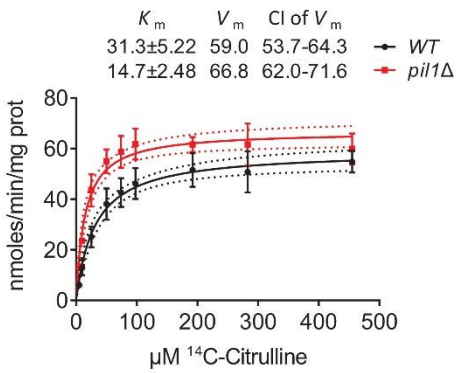

Figure 3.11 Gap1 kinetic characteristics in cells lacking EMC/eisosomes

Concentration-dependent kinetics of [^{14}C]Cit uptake in a *WT* and a *pil1*Δ strain. Error bars indicate SD; n = 2. Analysis and representations are as in Fig. 2.10 a. F-pvalue of Vmax = 0.0313; F-pvalue of Km = 0.0024.

As further evidence that EMC residency does not modulate transporter activity, the kinetic characteristics of EMC-bound Can1 were measured. A GFP-binding protein domain (GB) (Rothbauer *et al.*, 2008; for a review of applications see Schumacher *et al.*, 2018) was translationally linked to Sur7, which is found exclusively in the EMC. This way, when Can1-GFP is coexpressed, the majority of Can1 molecules are attracted to EMC patches and retained there by relatively stable interactions with the GB. Sur7 localization is not affected in any way, even upon addition of arginine, when bound Can1 should exit EMCs. Conversely, Can1 remains mostly bound to Sur7 via the linked GB domain and thus

enriched in EMCs. This was later confirmed quantitatively by confocal microscopy (Gournas *et al.*, 2018). Kinetic analysis in these conditions revealed no difference in either

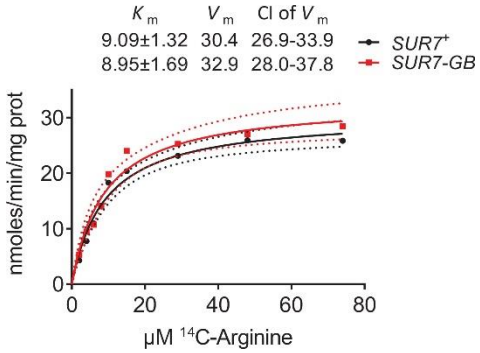

Figure 3.12 Trapping Can1 in EMCs does not affect its activity

Concentration-dependent kinetics of [^{14}C]Arg uptake in a *WT* and a *SUR7-GB* (*gap1*Δ *can1*Δ) strain expressing Can1-GFP under its native promoter. Analysis and representations are as in Fig. 2.10 a. F-pvalue of Vmax = 0.3327; F-pvalue of Km = 0.9453.

the apparent K_m or V_{max} of Can1 (Figure 3.12).

3.6. Trapping Can1 in EMCs causes a marked decrease in transporter endocytosis and degradation

Given that the levels of Can1 are constitutively lower in cells lacking EMC/eisosomes and that EMC exit seems to precede the substrate-induced ubiquitination and endocytosis of Can1, it was tested whether EMCs have a protective effect on Can1.

This was tested by trapping Can1 in the EMCs using the Sur7-GB construct in conditions where Can1 endocytosis is normally promoted. Indeed, in a strain expressing this construct, vacuolar degradation of Can1 upon arginine addition is significantly reduced (Figure 3.13). This effect was later shown to be lost in a *pil1*Δ strain even when co-expressing Sur7-GB to rule out an effect from GB binding (Gournas *et al.*, 2018). These results suggest that EMC/eisosomes protect Can1 form endocytosis *in vivo*, potentially by rendering the transporter molecules inaccessible for ubiquitination.

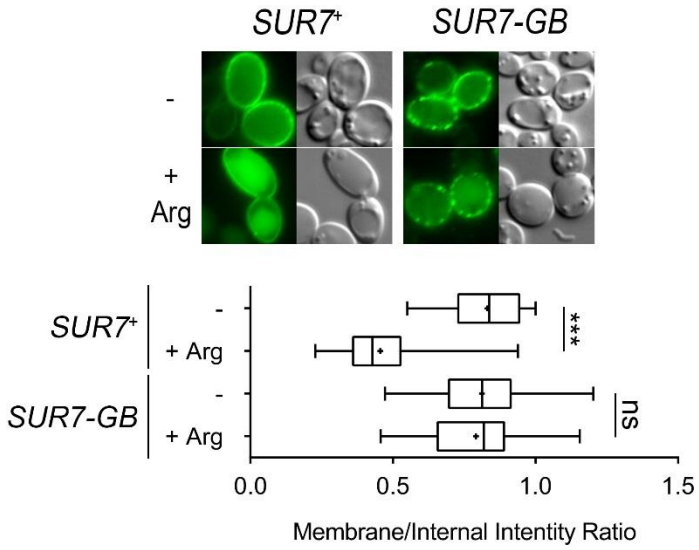

Figure 3.13 Trapping Can1 in EMCs protects it from substrate-induced endocytosis

Wide field epifluorescence microscopy of Arg-induced endocytosis of Can1-GFP in *WT* and *SUR7-GB* cells (*PIL1-mCherry gap1*Δ *can1*Δ), grown in Raf Pro medium. Gal was added for 1 h, and then Glu was added for 1.5 h. Quantification of PM/Internal fluorescence intensity (n = 50 cells) is as in Fig. 2.4. ***, P < 0.001; ns, nonsignificant, P > 0.05.

Despite showing that EMCs protect Can1 from endocytosis, the conditions under which this is physiologically significant were unclear. Given the dynamic localization of Can1, this function could be served only in conditions under which the transporter is normally in the EMCs. As shown previously, Can1 exits EMCs when it is active and transports arginine. Also, specificity in substrate-induced endocytosis is already achieved, at least for Can1, by the combined requirement for Art1 and Rsp5 activation and exposure of the Art1BS which is coupled to transporter activity (See Introduction). So, any physiological significance would be exhibited in the absence of its substrate. More specifically, nutrient starvation is known to promote the degradation of many proteins including transporters. This is also the case for nitrogen starvation, where TORC1 is inhibited, an effect that is mimicked by rapamycin. This Rap-induced TORC1 inactivation has already been shown to promote the ubiquitination and internalization of several permeases including Can1 (Crapeau, Merhi and André, 2014). Under these conditions, it might be favorable to preferentially retain a fraction of nutrient transporters, in order to promote more efficient growth recovery when nutrients become available.

The next step was to test whether this also holds for other EMC-enriched amino acid permeases. In contrast, deletion of EMC/eisosomes should have no effect on transporters, like Gap1, which are uniformly distributed on the PM. The same protective effect was observed for Lyp1, in addition to Can1, but, importantly, not for Gap1 (Figure 3.14). Interestingly, the effect on Gap1 was actually reversed, but this slight protection in *pil1*Δ cells can be explained by taking into account the general defect in endocytosis caused by the lack of eisosomes (See Introduction). This has been suggested to occur because the lack of invaginations allows the cortical ER to reach closer to the membrane, thus hindering the formation of endocytic sites. These preliminary results were later confirmed by measurement of the initial uptake rate of the transporters, in the absence of Rap compared to treated cells (Gournas *et al.*, 2018).

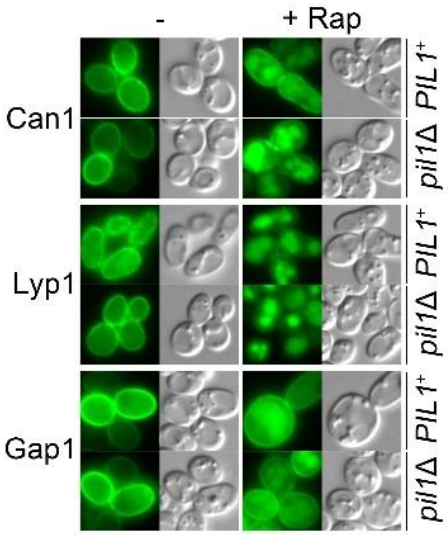

Figure 3.14 EMC-encriched Can1 and Lyp1 are differentially protected from Rap-induced endocytosis

Wide field epifluorescence microscopy of *WT* and *pil1*Δ (*gap1*Δ *can1*Δ) cells expressing Can1-GFP, Lyp1-GFP or Gap1-GFP. Cells were grown in Gal Pro medium and treated or not with 200 ng/mL Rap for 3 h.

4. Discussion

This thesis started with the goal of following up on observations regarding the ubiquitination status and the lateral segregation of Can1 made in the course of a previous project in the lab that focused on the arrestin-mediated downregulation of Can1. Here, the lateral segregation of Can1 is shown to be independent of its ubiquitination. The 7KR mutant, and Can1 in the *art1*Δ, *bul1/2*Δ strain are preferentially enriched in EMC and this is lost upon addition of Arg, indistinguishable from WT Can1. The same phenotype is obtained by hypo-expressing the Rsp5 ligase (Gournas *et al.*, 2018). Can1 exits EMC/eisosomes when it transports its substrate, due to a conformational change from an OF to an IF state. This offers a substrate specific mechanism to deplete EMCs of active transporters. Notably, as shown later, Can1 exits EMC also upon addition of lysine, as it transports it at a slower rate (Ghaddar, Krammer, *et al.*, 2014), and the lysine-converted Can1(S176N,T456S) mutant only responds to lysine (Gournas *et al.*, 2018). This conformational shift is mimicked constitutively by the Can1(E184Q) mutant, that is predicted to be blocked in the IF state. Intact sphingolipid biosynthesis is required for the preferential segregation of Can1 to EMCs, providing further evidence that the compartment could be enriched in sphingolipids. FRAP analysis later showed that Can1 diffuses slower in EMCs and that this depends both on intact sphingolipid biosynthesis and the conformation state of the transporter (Gournas *et al.*, 2018), also indicating a potential interaction of Can1 with SLs in it OF state. Lastly, EMC-localization seems to protect resident transporters from endocytosis under nitrogen starvation, a condition with physiological significance, as it could allow faster resumption of growth upon nutrient availability. Recently, the role of EMC/eisosome enlargement in nutrient starvation was linked with this observation (Gournas *et al.*, 2018). The larger area covered by the domain in late stationary phase enhances the protective effect it exerts on resident permeases (Figure 4.1).

These results are largely in agreement with a study on Mup1 (Wedlich-Söldner *et al.*, 2018, pre-print), where they find the same conformation-dependence and further show that its distribution outside the EMC forms a disperse network, as expected from the

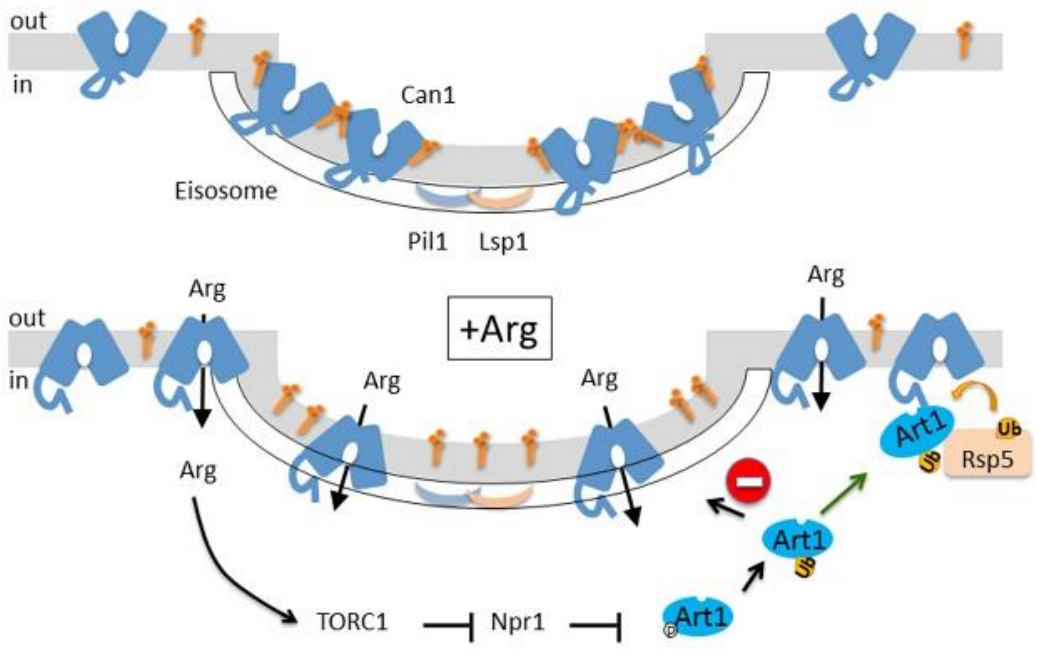

Figure 4.1 Summary of the model proposed for the EMC-enrichment of Can1 and its substrate-induced ubiquitination

In the absence of Arg Can1 preferentially clusters in EMC/eisosomes, possibly due to interactions with sphingolipids in its OF state. Upon transport of Arg, Can1 shifts transiently to an IF conformation, which lacks the increased affinity for EMCs and exposes the Art1BS. Intracellular Arg leads to Art1 activation through TORC1. Can1 becomes homogeneous in the PM, increasing the chance of ubiquitination from the Art1/Rsp5 complex, since EMC-localization renders Can1 inaccessible. Under nutrient starvation, this protective effect leads to retention of a larger fraction of resident transporters for quicker resumption of growth.

current consensus on plasma membrane organization. Mup1 is also protected from endocytosis, while its activity remains normal. However, their hypothesis implicating the C-terminal tail in the localization mechanism, based on the homogenous distribution of a mutant lacking a portion of its C-terminal tail is puzzling, as the same does not seem to hold for Can1 (Unpublished observations). Since, however, Mup1 belongs to the L-type Amino Acid Transporter (LAT) family, determinants could actually be distinct.

A recent study in mammalian cells implicates the surface area, length and palmitoylation of transmembrane domains (TMDs) of proteins, as determinants of their association with membrane rafts (Lorent *et al.*, 2017). Even though Can1, in contrast with some other EMC-resident transporters, has been shown to not be palmitoylated (Popov-Čeleketić *et al.*, 2016) and no discernible pattern can be observed for this modification, a similar

mechanism could govern EMC presence and/or enrichment based on the similarities between EMCs and rafts which are mesoscopic domains with a distinct, more ordered lipidic composition (Klose *et al.*, 2010). This provides an interesting scenario where, a conformational change as part of the transport cycle could also change the total area covered by Can1 in one or both leaflets, thus modifying its affinity for the EMC. Alternatively, Can1 could directly interact with specific lipidic species also enriched in the EMC and lose this interaction in a different conformation. Based on the relationship between the EMC and complex sphingolipids (discussed below) and also a study reporting a specific sphingolipid binding motif on a mammalian monospan protein (Contreras *et al.*, 2012), we tried to look for patterns in the presence of this motif in membrane proteins of known localization, mostly focusing on nutrient permeases and the well-studied Nce102 and Sur7 but were unable to produce any results. This scenario however remains to be studied further. Notably, quite recently, a sterol-interaction motif was characterized in a mammalian transporter that regulates transitions between conformations (Zeppelin *et al.*, 2018).

We showed that we have indeed decoupled the ubiquitination status of Can1 from its plasma membrane localization as two separate phenomena, and going further, that Can1 is inaccessible to the ubiquitination machinery of the cell while at the EMC. It remains unclear whether ubiquitinated Can1 is able to enter the EMC normally, or if it would be excluded possibly due to steric hindrances. Previous studies have ruled out involvement of the actin cytoskeleton in the formation and maintenance of EMC/eisosomes (Malínská *et al.*, 2004), but this role could be served by the Pil1/Lsp1 protein coat. Very recently, the size of the cytoplasmic domains of a protein was proposed as the main determinant of EMC presence (Bianchi *et al.*, 2018). According to this model, Can1 in contrast with Pma1 is able to enter the EMC and for unknown reasons a subpopulation may become 'trapped' there. Thus, the added volume of the ubiquitin molecules could prevent modified Can1 from re-entering the EMC, but this remains a perspective. The authors also suggest that there is a limited number of 'traps' for proteins like Can1 and the enrichment is due to these few immobile molecules and not to a generally slower diffusion rate in the

compartment. They support this by the fact that overexpression of Can1 leads to a decrease in the EMC/non-EMC ratio of Can1, indicating that the capacity of the EMC is exceeded. However, in a later experiment done in the lab, the FRAP half-life constant of Can1 in EMCs was shown to be increased as compared with the rest of the cell membrane, even when overexpressing Can1 under the *GAL* promoter (Gournas *et al.*, 2018; Unpublished lab observations). Since the number of Can1 molecules in EMCs increases, while their diffusion rate remains decreased, this may be interpreted to contradict their model of a limited, saturated number of 'traps'. These results fit better with a homogeneous decrease in the lateral diffusion rate in EMCs, possibly due to specific interactions with EMC lipids or a very abundant protein. However, given the multitude of parameters, their general model of temporal trapping of individual molecules that lead to a macroscopic slower diffusion rate is highly compatible with our results.

The mechanism of the enrichment of Can1 and other proteins in the EMC remains unknown. Although the link between the EMC and sphingolipid sensing and biosynthesis is well established, evidence for their presence in the compartment have not been produced. In later works, the EMC enrichment of Can1 was found to be independent of Nce102 (Gournas *et al.*, 2018), which was suspected to be responsible for this phenomenon mainly because of its implication in sphingolipid sensing. A direct interaction with sphingolipids or another EMC-concentrated lipid remains a promising alternative theory. The study of protein-lipid interactions is still an emerging field (Saliba, Vonkova and Gavin, 2015), and the regulation of protein structure and function by direct interaction with sphingolipid molecules has been demonstrated (Contreras *et al.*, 2012). A computational and later mutational attempt to apply their findings on our proteins of interests was fruitless (See Discussion on Conformational Change). We were only able to show that intact sphingolipid biosynthesis is required. Later FRAP analysis provides further evidence that SL biogenesis is required for the preferential segregation of Can1 in EMCs. In these experiments, Can1 exhibited slower diffusion in EMCs, which was lost both upon addition of Arg and sustained SL biogenesis inhibition (Gournas *et al.*, 2018).

In regard to the physiological significance of EMC/eisosomes, they seem to also play a role in nutrient starvation conditions. Earlier experiments have shown that the invaginations of the plasma membrane increase both in number and in size in stationary phase (Takeo, Shigeta and Takagi, 1976; Walther, Müller and Schweingruber, 1984). This process was recently shown for EMC/eisosomes to be regulated by Lsp1, the role of which had remained elusive (Gournas *et al.*, 2018). The main EMC/eisosome components Pil1, Lsp1, Nce102 and Sur7 were also shown to increase threefold in membrane enriched extracts of cells shifted to a poor nitrogen source (Villers *et al.*, 2017). There are more ways in which the protective effect of EMC/eisosomes can be modulated. Upon nutrient starvation, the diffusion rate of Can1 in EMCs is reduced, thus accentuating the phenomenon (Gournas *et al.*, 2018). Thus, EMC-enriched transporters are protected from endocytosis and degradation in these conditions, an effect which is mimicked by rapamycin. This is important both for resumption of growth upon favorable conditions and also, potentially, for growth in nutrient-scarce conditions. Several other reports link EMC/eisosomes with a response to nutrient starvation. Notably, Xrn1, the main mRNA decay enzyme, is known to accumulate to EMCs in response to glucose exhaustion, which correlates with decreased activity (Grousl *et al.*, 2015; Vaškovičová *et al.*, 2017). The results together reinforce the notion that EMC/eisosomes are dynamic, tightly regulated structures with a variety of roles. The understanding of these fungal specific structures, could provide insights into analogous roles of regulation at the plasma membrane, and allow the development of new antifungal drugs.

5. Materials and Methods

5.1. Yeast Strains

All *S. cerevisiae* strains used in this study are derived from the Σ1278b wild isolate. Strains used in the results section of this study are shown in Table 5.1.

Table 5.1

Strain	Genotype	Reference
23344c	*ura3*	Laboratory collection
EK008	*gap1Δ ura3*	Laboratory collection
CG014	*SUR7-mRFP art1Δ ura3*	Laboratory collection
MYC011	*sur7Δ gap1Δ ura3*	Laboratory collection
ES029	*gap1Δ can1Δ ura3*	Gournas *et al.*, 2017
ES031	*art1Δ can1Δ gap1Δ ura3*	Gournas *et al.*, 2017
ES032	*can1Δ ura3*	Gournas *et al.*, 2017
MYC013	*pil1Δ gap1Δ ura3*	Gournas *et al.*, 2018
CG050	*can1Δ pil1Δ gap1Δ ura3*	Gournas *et al.*, 2018
CG056	*pil1Δ ura3*	Gournas *et al.*, 2018
SG001	*PIL1(4A)-GFP can1Δ SUR7-mRFP gap1Δ*	Gournas *et al.*, 2018
SG023	*PIL1(4A)-mRFPmars can1Δ gap1Δ ura3*	Gournas *et al.*, 2018
SG035	*PIL1-mCherry gap1Δ can1Δ ura3*	Gournas *et al.*, 2018
SG041	*PIL1-mCherry art1Δ can1Δ bul1Δ bul2Δ gap1Δ ura3*	Gournas *et al.*, 2018
SG067	*SUR7-GB PIL1-mCherry gap1Δ can1Δ ura3*	Gournas *et al.*, 2018

5.2. Oligos – PCR Primers

Oligos used in PCR for the construction of transformation cassettes or for verification of sequences are listed in Table 5.2.

Table 5.2

Nb	Primer name	Sequence (5'-3')
1	D5 art1	tcctacttagtatacatttcactaaacaatacgttttaccgcggccgccagctgaagctt
2	D3 art1	aatatatggtaaatacctttaacgaatattataaaatctagcggccgcataggccactag
3	V5 art1	gctttttcggaggagaacgc
4	V3 art1	agttttgggatggatggtcc
5	D5 pil1	tattgcaaagtgaagaatatatcagcatcaagtatatagtgcggccgccagctgaagctt
6	D3 pil1	ttttttttgtttctaatagattgttgatttattttgattagcggccgcataggccactag
7	V5 pil1	gttgattatcccaacccaag
8	pil1-V3ext	ctaaagtaaggagtgaggag
9	S3-pil1-5GA	gtcggacaccagcaaagtgagtctcttccccaacaaacaacagctggagcaggtgctggtgctggtgctggagcacgtacgctgcaggtcgac
10	S2-pil1	gctggtttttttttttttgtttctaatagattgttgatttattttgaatcgatgaattcgagctcg
11	pil1-V5int	gaagacgaacaagaagatgg
12	Sur7-S3 for	cttcttcactataagaaaatcacacgagcgcccggacgatgtctctgttcgtacgctgcaggtcgac
13	Sur7-S2 rev	gagagaagaaaggggtataaatatatattacaaagcggaaaacttgcgccatttaatcgatgaattcgagctcg
14	sur7-V5ext	cagcaatggtctaggtagtg
15	sur7-V3ext	gacattttgaggtcgttcgg
16	pil1-MARS DJp2	aagcttcagctggcggccgcgataagcttttaagcgcctg
17	pil1-MARS DJp3	caggcgcttaaaagcttatcgcggccgccagctgaagctt
18	Upstream of T7	gaccgagcgcagcgagtcag
19	pil1- DJP1 nested	gtctcacatctgcatctgcacatttatttacc

5.3. Plasmids

The plasmids used in this study are listed in Table 5.3. All derive from the centromere-based pFL38 vector carrying the *URA3* gene, except as otherwise noted.

Table 5.3

Plasmid	Description	Ref. or source
pFL38	CEN-ARS (URA3)	Bonneaud *et al.*, 1991
pJOD10	CEN-ARS GAL1-GAP1-GFP (URA3)	Nikko, Marini, André, 2003
pNAM001	CEN-ARS LYP1-GFP (URA3)	Ghaddar *et al.*, 2014a
pKG036	CEN-ARS CAN1-GFP (URA3)	Ghaddar *et al.*, 2014a
pCJ563	CEN-ARS GAL1-CAN1-GFP (URA3)	Ghaddar *et al.*, 2014a
pCJ560	CEN-ARS GAL1-CAN1(E184Q)-GFP (URA3)	Gournas *et al.*, 2017
pCJ574	CEN-ARS GAL1-CAN1(E184A)-GFP (URA3)	Gournas *et al.*, 2017
pCJ565	CEN-ARS GAL1-CAN1(T180R)-GFP (URA3)	Gournas *et al.*, 2017
pCG030	CEN-ARS GAL1-CAN1(S176N,T456S)-GFP (URA3)	Gournas *et al.*, 2017
pCG032	CEN-ARS GAL1-CAN1(S176N)-GFP (URA3)	Gournas *et al.*, 2017

pCJ570	CEN-ARS GAL1-CAN1(T456S)-GFP (URA3)	Gournas *et al.*, 2017; as pCJ569
pCG080	CEN-ARS GAL1-CAN1(K5R,K13R,K42R,K45R,K47R,K85R,K89R)-GFP (URA3)	Gournas *et al.*, 2017
pCG025	CEN-ARS GAL1-CAN1(ELK89-AAAA)-GFP (URA3)	Gournas *et al.*, 2017
pCG106	CEN-ARS GAL1-CAN1(K5R,K13R,K42R,K45R,K47R,K85R,K89R,E184Q)-GFP (URA3)	Gournas *et al.*, 2018
pRS306-pil1_GFP Nr::6	PIL1(S45A,S59A,S230A,T233A)-GFP (URA3)	Walther *et al.*, 2007
pRS306_pil(4A)-MARS	PIL1(S45A,S59A,S230A,T233A)-mRFPmars (URA3)	Walther *et al.*, 2007
pYM42-GFP Chromobody-NatR	GFP Chromobody-NatR (URA3)	Wedlich-Söldner's lab collection

5.4. Yeast Growth Media and Conditions

Cells were cultured at 29 °C either in YPD rich medium, or synthetic minimal medium (Jacobs, Jauniaux and Grenson, 1980). Liquid media were solidified by addition of 0.9-1% agarose.

	YPD Medium (per 1 L)
Yeast Extract	10 g
Bactopeptone	10 g
Glucose	20 g

The synthetic minimal medium was prepared by mixing the following solutions, all previously sterilized. All solutions were sterilized at 121 °C, except for urea and the trace metals solution, which were filtered. The salts solution was adjusted to pH 6.1 with further addition of KOH.

	Synthetic Minimal Medium (per 1 L)
Salts solution	Approximately 800 mL, after sterilization of 1 L
Trace Metals solution	1 mL

Vitamins solution	10 mL
Carbon source	To final concenctration: glucose (3%) or galactose (3%) + glucose (0.3%) or raffinose (3%)
H_2O	To 1 L
Nitrogen source	To final concentration: $(NH4)_2SO_4$ (10 mM) or proline (10 mM) or urea (5 mM)

Salts solution	**1 L**	**Trace Metals solution**	**1 L**	**Vitamins solution**	**1 L**
$MgSO_4 \cdot 7\ H_2O$	0.7 g	**H_3BO_3**	10 mg	**D-biotin**	150 µg
KH_2PO_4	1 g	**$CuSO_4 \cdot 5\ H_2O$**	1 mg	**Thiamin · HCl**	100 mg
$CaCl_2 \cdot 2\ H_2O$	0.4 g	**KI**	2 mg	**Inositol**	1 g
NaCl	0.5 g	**$Na_2MoO_4 \cdot 2\ H_2O$**	4 mg	**D-Calcium pantothenate**	200 mg
Citric acid · H_2O	10.5 g	**$ZnSO_4 \cdot 7\ H_2O$**	14 mg	**Pyridoxine · HCl**	100 mg
10 M KOH	16 mL	**Citric acid · H_2O**	10 g		
		$MnSO_4 \cdot H_2O$	400 mg		
		$FeCl_3 \cdot 6\ H_2O$	5 g		

For selection of resistant *S. cerevisiae* colonies, antibiotics were used in the following concentrations: Geneticin (G418) 200 µg/mL, Nourseothricin (NTC) 200 µg/mL. The final concentrations of substances added to solid or liquid media were Arg (5 mM), Lys (5 mM), Myr (10 µM) and Rap (200 ng/mL).

5.5. *S. cerevisiae* strain storage

Strains can be stored for extended periods of time in 15% glycerol at -80 °C. Single colonies were picked to inoculate liquid minimal medium and grown to mid-log phase. Approximately 0.75 mL of culture were mixed with equal volume of 30% glycerol in 2.0 mL cryogenic tubes and stored at -80 °C. To recover a strain from a stock, cells are scraped and streaked on appropriate solid medium without thawing the tube.

5.6. Bacterial growth media

JM109 strain *Escherichia coli* cells were grown in customized Terrific Broth (TB) medium.

	TB Medium (per 1 L)
Yeast Extract	23.6 g
Peptone	11.8 g
K_2HPO_4	9.4 g
KH_2PO_4	2.2 g

5.7. Preparation of electrocompetent bacterial cells

A single colony of JM109 cells was used to inoculate 500 mL of TB liquid medium and incubated overnight at 37 °C with agitation. A total of 45 mL of culture was used to inoculate 4.5 L of TB distributed to nine 1 L flasks and incubated for 3 h at 37 °C with agitation. Cells were collected in six 250 mL bottles by sequential centrifugations at 4 °C at 7,000 rpm. The supernatants were discarded and the pellets resuspended in 10 mL of frozen 5% glycerol, then transferred to four 50 mL tubes and centrifuged for 10 min at 9,000 rpm and 4 °C. The pellets were resuspended in 15 mL of cold 5% glycerol each and transferred to two 50 mL tubes. After another centrifugation for 10 min at 9,000 rpm and 4 °C and elimination of the supernatant, cells were resuspended in 20 mL cold 10% glycerol followed by another centrifugation as previously. The supernatant was again discarded and all the cells resuspended in 9 mL cold glycerol (final volume approximately 18 mL). Finally, 45 µL aliquots were made in 1.5 mL Eppendorfs and stored at -80 °C.

5.8. Transformation of *E. coli* by electroporation

Bacterial transformations were performed using a Bio-Rad electroporator as follows: a few microliters of dialyzed total DNA extract from yeast were added to 45 µL of

electrocompetent cells at 4 °C, mixed, and transferred to cold electroporation cuvettes containing 1 mL of TB medium. Cuvettes were previously sterilized with 100% ethanol and cooled and dried in vacuum. After electroporation, cells were transferred to 1.5 mL Eppendorfs and incubated for 1 h at 37 °C, centrifuged for 2 min at 8,000 rpm, resuspended in sterile water and spread on solid TB medium supplemented with ampicillin 100 µg/mL for selection. A negative control without added DNA was always included to check for contaminations.

5.9. Plasmid DNA isolation from *E. coli* cells

For this procedure, a Thermo Scientific GeneJET Plasmid Miniprep Kit was used as recommended in the manufacturer's protocol. Plasmid yield was assessed by electrophoresis on agarose gel.

5.10. Total DNA extraction from *S. cerevisiae* cells

The following is a slight alteration of the procedure described by (Lööke, Kristjuahan and Kristjuhan, 2011). Streaked yeast colonies were suspended in 100 µL 200 mM lithium acetate (LiOAc); 1% SDS solution, vortexed and incubated for 5 min at 70 °C. Starting with the next step, all procedures were carried out at 4 °C. 300 µL of 100% ethanol were added for DNA precipitation, samples were mixed by brief vortexing and DNA was collected by centrifugation (15,000 × g for 5 min). Supernatant was removed and the pellet was washed with 1 mL 70% ethanol, left for 5-10 min to evaporate remaining ethanol at 55 °C and then suspended in either 100 µL (for PCR) or 15 µL (for dialysis) water to dissolve DNA. The debris was removed by centrifugation (15,000 × g for 5 min) and 1 µL supernatant was used for PCR or as much as possible for dialysis.

5.11. DNA dialysis for electroporation

Dialysis of extracted yeast DNA is required before electroporation to remove excess salts that decrease efficiency. About 7 µL drops of DNA were laid on 0.025 µm Millipore filters floating on distilled water. The samples were retrieved after 10 min, transferred to new 1.5 mL Eppendorfs and stored at -20 °C.

5.12. DNA digestion with restriction enzymes

Restriction enzymes were sometimes used to identify of verify plasmids, as per manufacturer's instructions.

5.13. Transformation of *S. cerevisiae*

As previously discussed, yeast cells are capable both of integrating DNA into their genome by homologous recombination and retaining replicative plasmids. The same rapid, low-yield transformation protocol is used for both procedures (Adapted from Gietz and Schiestl, 2007). A single, fresh colony was used to inoculate 5 mL of rich medium and incubated for several hours to early log phase. This was used to inoculate 50 mL of rich medium to OD_{660} 0.5 after overnight incubation. Cells were then pelleted by centrifugation for 4 min at 3,000 rpm, resuspended in 1 mL sterile water, transferred to a 2.0 mL Eppendorf, centrifuged for 30 s, resuspended again in 1 mL water, centrifuged for 30 s, resuspended in 1 mL TE/LiAc solution, centrifuged for 30 s and finally resuspended in 0.5 mL TE/LiAc. The following were added to 50 µL cell suspension, in order: 1) 5 µL boiled salmon sperm DNA (10 mg/mL), mixed gently, 2) approximately 1 µg DNA to transform, mixed gently, 3) 300 µL TE/LiAc/ 40% PEG solution, then homogenized. The mixture was incubated for 30 min at 29 °C followed by a thermal shock for 15 min at 42 °C. Finally, cells were collected by centrifugation (15,000 × g for 1 min) and washed once with 1 mL water. When transforming with a replicative plasmid, cells were resuspended in 100 µL and usually spread on solid synthetic minimal medium to select for uracil prototrophy. For integration to the genome, cells have to be grown for 4 h in non-selective rich medium and then usually transferred to solid rich medium complemented with the appropriate antibiotic.

	Composition
TE/LiAc	0.1 M LiAc pH 7.5, 10 mM Tris pH 7.5, 1 mM EDTA pH 7.5
TE/LiAc/40% PEG	TE/LiAc + 40% Polyethylene glycol (PEG) 4000

5.14. Polymerase Chain Reactions

PCR were carried out according to the polymerase manufacturer's instructions. For high quality amplifications, i.e. when the products were used for transformations or sequencing for verification, a proof-reading Q5® High-Fidelity DNA Polymerase was used (NEB). When simply verifying a transformation by checking the length of a product, either a OneTaq® DNA Polymerase (NEB) or a GoTaq® DNA Polymerase (Promega) was used according to the following protocols:

Primer T_ms were calculated using the NEB Tm Calculator for Q5® and OneTaq®, and the following empirical expression for GoTaq®:

69.3 + 0.41 * GC% - 650/Length

Annealing temperatures were calculated as follows, based on the T_m of the primer which is lower:

For Q5® and OneTaq®: Using the NEB T_m Calculator

For GoTaq®: $T_a = T_m\_lower + 3$ °C

	Q5® High-Fidelity	**OneTaq®**	**GoTaq®**
Reaction Buffer	1x	1x	1x
PCR Nucleotide Mix	0.2 mM each	0.2 mM each	0.2 mM each
Upstream primer	0.5 µM	0.2 µM	0.1–1.0 µM
Downstream primer	0.5 µM	0.2 µM	0.1–1.0 µM
DNA Polymerase	0.02 U/µl	0.025 U/µl	0.025 U/µl
Template DNA	< 200 ng/µl	< 200 ng/µl	< 500 ng/µl
Nuclease-Free Water	To 25 or 50 µl	To 25 µl	To 25 µl

Step	**Q5® High-Fidelity**	**OneTaq®**	**GoTaq®**
Initial Denaturation	98 °C 30 s	94 °C 30 s	95 °C 2 min
Denaturation	98 °C 10 s	94 °C 30 s	95 °C 0.5–1 min
Annealing	T_a 30 s	T_a 15-60 s	T_a 0.5–1 min
Extension	72 °C 30 s/kb	68 °C 1 min/kb	72 °C 1 min/kb
Cycling (Steps 2-4)	35 cycles	25-30 cycles	25-30 cycles

Final Extension	72 °C 2 min	68 °C 5 min	72 °C 5 min	
Hold	4–10 °C	4-10°C	4 °C	
Product		Primer pair	Expected size (bp)	T_a (°C)
G418* for *art1Δ		1, 2	1600	72
G418* for *pil1Δ		5, 6	1600	72
mCherry-G418* for *PIL1-mCherry		9, 10	4900	63
GB-G418* for *SUR7-GB		12, 13	1700	63
PIL1(4A)-mRFPmars		7, 16	1800	61
NatR		17, 18	1500	72
***PIL1(4A)-mRFPmars-NatR* cassette**		19, 6	3100	70

Product	**Primer pair**	**Expected size if successful (bp)**	**Expected size if failed (bp)**	**T_a (°C)***
art1Δ::G418	3, 4	4600	3000	53/60
pil1Δ::G418	7, 8	3000	1400	46/58
PIL1-mCherry-G418	11, 8	5200	300	46/58
SUR7-GB-G418	14, 15	3100	1400	50/60
PIL1(4A)-mRFPmars-NatR	11, 8	2400	-	46/58

*Indicated temperatures are for GoTaq® and OneTaq®, respectively.

5.15. DNA constructs for genomic integrations

Construction of the *ART1* deletion sequence

The *loxP–kanMX–loxP* disruption cassette conferring resistance to G418 was PCR amplified using primers 1 and 2 from the pUG6 plasmid (Güldener *et al.*, 1996). These chimeric primers include 40-45 bp from the 5' and 3' UTR respectively of the *ART1* gene to induce integration on the *ART1* locus of by homologous recombination. The resulting amplified DNA construct was used to transform a *can1Δ::HgB bul1Δ::G418S bul2Δ::G418S gap1Δ::G418S ura3* strain, selecting for G418 resistance. Candidates were verified by PCR using primers 3 and 4, which flank the *ART1* locus outside where primers 1 and 2 bind.

Construction of the *PIL1* deletion sequence

The *loxP–kanMX–loxP* disruption cassette conferring resistance to G418 was PCR amplified using primers 5 and 6 from the pUG6 plasmid. These chimeric primers include 40 bp from the 5' and 3' UTR respectively of the *PIL1* gene to induce integration on the *PIL1* locus of by homologous recombination. The resulting amplified DNA construct was used to transform a *gap1*Δ*::G418S can1*Δ*::G418S art1*Δ*::HgB ura3*, a *can1*Δ*::G418S gap1*Δ*::G418S npi1-1 ura3* and a *can1*Δ*::HgB bul1*Δ*::G418S bul2*Δ*::G418S gap1*Δ*::G418S ura3* strain, selecting for G418 resistance. Candidates were verified by PCR using primers 7 and 8, which flank the *PIL1* locus outside where primers 5 and 6 bind.

Rescue of the G418 resistance selection marker using the Cre/*loxP* system

The Cre recombinase was sometimes used to excise selection genes flanked by *loxP* sites by homologous recombination between the two sites, to facilitate multiple gene knock-outs. For this purpose, strains were transformed with the pSH47 plasmid carrying the *cre* recombinase gene under the control of the *GAL1* promoter (Güldener *et al.*, 1996) and selected for uracil prototrophy. Transformants were transferred to YPGal liquid medium and cultured overnight to induce Cre expression, then streaked on YPD medium to isolate single colonies. Replica-plating of colonies on YPD plus G418 confirmed excision of the marker. In order to abolish the plasmid, 5-fluoroorotic acid (5-FOA), which is metabolized to a toxic uracil analog (5-fluorouracil or 5-FU) by Ura3, was added to minimal medium plus uracil, positively selecting for the loss of the *URA3*-containing plasmid pSH47.

Construction of a sequence for the translational fusion of mCherry with Pil1 in the *PIL1* locus

A cassette containing yomCherry at its 5' end followed by the *kanMX4* module conferring G418 resistance for translational fusion with the *PIL1* gene was amplified using primers 9 and 10 with the addition of a 5xGA linker, from the genomic DNA of a strain expressing Sec7-yomCherry from the laboratory collection, according to published instructions (Janke *et al.*, 2004). The resulting amplified DNA was used to transform a *gap1*Δ*::G418S ura3*, a *gap1*Δ*::G418S can1*Δ*::G418S ura3*, a *gap1*Δ*::G418S can1*Δ*::G418S art1*Δ*::HgB ura3*, a *can1*Δ*::HgB bul1*Δ*::G418S bul2*Δ*::G418S gap1*Δ*::G418S ura3*, a *art1*Δ*::G418S*

can1Δ::HgB bul1Δ::G418S bul2Δ::G418S gap1Δ::G418S ura3 and a *can1Δ::G418S gap1Δ::G418S npi1-1 ura3* strain. Transformants were selected for resistance to G418 and verified using primers 11, which binds inside the *PIL1* ORF and 8, which flanks the *PIL1* locus outside where primer 10 binds.

Construction of a sequence for the translational fusion of the GFP-binder with Sur7 in the *SUR7* locus

A cassette containing the GFP-binder at its 5' end followed by a nourseothricin resistance module was amplified using primers 12 and 13 from the pYM42-GFP Chromobody-NatR plasmid obtained from Dr. Wedlich-Söldner's lab, according to published instructions (Janke *et al.*, 2004). The resulting amplified DNA was used to transform a *gap1Δ::G418S can1Δ::G418S ura3*, a *gap1Δ::G418S can1Δ::G418S art1Δ::HgB ura3*, a *can1Δ::HgB bul1Δ::G418S bul2Δ::G418S gap1Δ::G418S ura3*, a *can1Δ::HgB pil1Δ::G418 gap1Δ::G418S ura3*, a *pil1Δ::G418 can1Δ::HgB bul1Δ::G418S bul2Δ::G418S gap1Δ::G418S ura3*, a *PIL1-mCherry-G418 gap1Δ::G418S can1Δ::G418S ura3*, a *PIL1-mCherry-G418 gap1Δ::G418S can1Δ::G418S art1Δ::HgB ura3*, a *PIL1-mCherry-G418 can1Δ::HgB bul1Δ::G418S bul2Δ::G418S gap1Δ::G418S ura3* and an *ART1-3xHA-G418 gap1Δ::G418S can1Δ::HgB ura3* strain. Transformants were selected for resistance to nourseothricin and verified using primers 14 and 15, which flank the *ART1* locus outside where primers 12 and 13 bind.

Integration of the plasmid carrying *PIL1(4A)-GFP* in the *URA3* locus

The pRS306-PIL1_GFP Nr.:6 plasmid (Walther *et al.*, 2007) containing the phosphorepressed mutant of Pil1, was integrated in the *URA3* locus by transforming a *pil1Δ::G418 can1Δ::HgB SUR7-mRFP-LEU2 leu2Δ::NatR gap1Δ::G418S ura3* and a *PIL1-mCherry-G418 gap1Δ::G418S can1Δ::G418S ura3* strain. Transformants were selected for uracil prototrophy on synthetic minimal medium.

Construction of a sequence for the integration of *PIL1(4A)-mRFPmars* in the *PIL1* locus

A cassette containing *PIL1(4A)-mRFPmars* followed by the *natMX4* resistance module was created in two pieces and joined using double-joint PCR (Yu *et al.*, 2004) as follows: *PIL1(4A)-mRFPmars* was PCR amplified from plasmid pRS306-pil1(4A)-Mars using primers 7 and 16. The *natMX4* module was PCR amplified from plasmid pAG25 using primers 17, the reverse complement of primer 16, and 18. As the two cassettes were complementary in the sequence of primers 16 and 17, they were used together as templates for a PCR in a 1/5 ratio, after gel extraction of the two cassettes. Primers used were 19 and 6. The final construct was used to transform a *can1Δ::HgB pil1Δ::G418 gap1Δ::G418S ura3* strain. Transformants were selected for nourseothricin resistance and confirmed with PCR using primers 11 and 8, which bind inside and outside the *PIL1* gene, respectively.

5.16. Radiolabeled amino acid uptake measurement and kinetic analysis

The apparent kinetic transport parameters were characterized by whole-cell uptake assays. Can1 and Gap1 transport activity was determined by measuring the initial uptake rate of [^{14}C]-labeled arginine or citrulline (PerkinElmer), respectively (Ghaddar, Krammer, *et al.*, 2014). Accumulated counts were measured 20 and 40 s after the addition of the radioactive substrate and corrected for protein concentration. Transport activity was expressed as nmol/mg of protein per unit of time and reported as the mean ± S.D. (n = 1-3). At least 9 substrate concentrations spread over a relevant range (2-100 µM Arg and 5-500 µM Cit) were used to determine the apparent Michaelis constant (K_m) and maximal velocity (V_{max}) values. The values were well fitted by a single-site Michaelis-Menten model. In contrast with the K_m, which is an intrinsic characteristic of a transporter, the V_{max} depends on the absolute quantity of transporter inserted into the membrane. Because this quantity depends on growth conditions and gene copy number, all uptake assays were carried out under the same, rigorously fixed conditions, so that the V_{max} values could be compared with each other. Data were analyzed using GraphPad Prism version 6.0.

5.17. Isolation and analysis of protein samples

Cells were grown to OD_{660} 0.2 in appropriate media.

5.18. Total protein extraction and isolation

Total cell protein extracts were isolated as follows (Adapted from Volland *et al.*, 1994): 5 mL were harvested by filtration and immediately stored at -80 °C. After resuspension in 0.5 mL water, they were lysed by addition of 50 µL NaOH 1 M and incubated for 10 min on ice. Proteins were precipitated by addition of 50 µL 50% TCA, a 10 min incubation on ice and centrifugation at 12,000 rpm for 5 min at 4 °C. The supernatant was discarded and the pelleted proteins resuspended in 100 µL sample buffer. All the above steps were carried out in cold conditions. Samples were heated to 37 °C for 10 min before loading.

	Composition
Sample Buffer	50 mM Tris-HCl pH 6.8, 2 mM EDTA, 2% SDS, 10% glycerol, 0.01% bromophenol blue, 0.5 M Tris, 2% β-mercaptoethanol

5.18.1. Isolation of membrane-enriched protein extracts

Briefly, 125-OD cells were filtered and frozen at −80 °C. The cells were washed with 5 mL TNE buffer [50 mM Tris · HCl (pH 7.4), 150 mM NaCl, 5 mM EDTA], resuspended in 2 mL TNE-I buffer [TNE supplemented with protease inhibitor mixture (Sigma) and 1 mM PMSF], and lysed with 800 µL glass beads by vortexing for 40 min at 4 °C. Cell debris was removed by a 4-min centrifugation at 500 × g and 4 °C, the supernatant was transferred to another tube, and crude membranes were pelleted by centrifugation at 16,100 × g and 4 °C for 90 min. Extracts of membrane-enriched preparations were resuspended in 100 µL TNE-I buffer. Protein concentrations were determined by Bradford's method.

5.18.2. Determination of protein sample concentration using the Bradford assay

In detergent resistance analysis, the concentration of protein needs to be determined so that the ratio of protein to Triton detergent falls within the analytic range. The Bradford method is a colorimetric assay based on the absorbance shift of an acidic solution of the Coomassie dye from 465 nm to 595 nm that occurs when it binds on proteins. The relation between absorbance at 595 nm and protein concentration is linear over a large range. A

standard curve was created by using known quantities of bovine serum albumin (BSA) and blinding was done with pure reagent. Protein sample concentration was determined by transferring 1-2 µL of sample to 2 mL of reagent, measuring its absorption at 595 nm and extrapolating the original sample concentration through the standard curve. Bradford reagent (Bio-Rad) was kept in cold storage and filtered just before use.

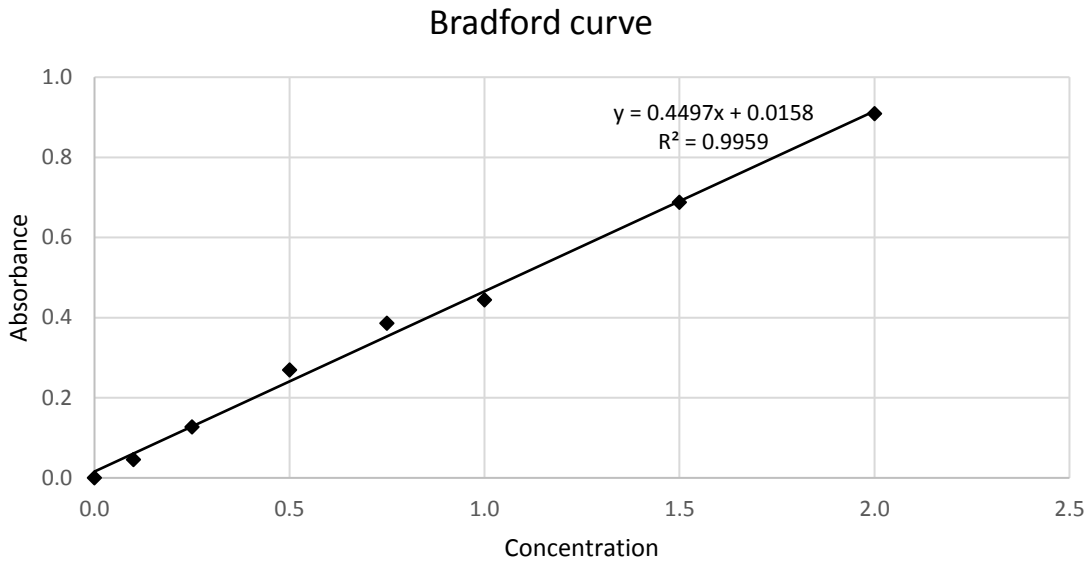

	Bradford's Reagent (1 L)
Coomassie Brilliant Blue G-250	100 mg
Ethanol	50 mL
85% (w/v) H_3PO_4	100 mL
H_2O	850

5.18.3. Detergent resistance analysis using Triton X-100

Determination of Can1 detergent resistance was performed as per Grossmann *et al.*, 2008. Aliquots of protein extracts from membrane-enriched preparations, corresponding to 30 µg protein, were treated at room temperature for 30 min with increasing

concentrations of Triton X-100 (0–0.8%) in a final volume of 60 µL TNE-I. The nonsolubilized material was pelleted by centrifugation (16,100 × g at 4 °C for 30 min) and washed with 100 µL. TNE-I buffer containing the corresponding concentration of Triton X-100. Pellets were resuspended in 30 µL sample buffer, dissociated at 90 °C for 2 min, resolved by SDS/PAGE, immunoblotted with anti-GFP antibody, and subsequently stripped and immunoblotted with anti-Gap1 and anti-Pma1 antibodies.

5.18.4. SDS-PAGE

Samples were analyzed by electrophoresis in a 9.2% SDS-polyacrylamide gel. Gel composition is described in the table below:

	Separation Gel (40 mL)	**Concentration Gel (10 mL)**
3 M Tris-HCl pH 8.45	15 mL	3.75 mL
40% Glycerol	15 mL	-
40% Acrylamide/Bisacrylamide (37.5/1)	9.2 mL	1.5 mL
10% (w/v) SDS	450 µL	150 µL
10% (w/v) APS	225 µL	112 µL
TEMED	22.5 µL	11.2 µL
H_2O distilled	5.4 mL	9.6 mL

Electrophoresis was carried out in a large-format Bio-Rad chamber at 30 V for one hour to concentrate the samples and then overnight at 90 V until the bromophenol dye reached the end of the gel to achieve better separation. The whole procedure was carried out under water cooling.

	Composition
Anode Buffer	0.2 M Tris-HCl pH 8.9
Cathode Buffer	0.1 M Tris-HCl, 0.1 M Tricine pH 8.25, 0.1% (w/v) SDS

5.18.5. Transfer of proteins to nitrocellulose membrane

After electrophoresis, a nitrocellulose membrane (Protran, Perkin Elmer) was placed on top of the gel, sandwiched between two 4-mm Whatman papers and placed in the transfer apparatus with the membrane facing the anode. Transfer was carried out in cold transfer buffer for 2 h at 85 V. After transfer, the membrane was washed with TBST until immunoblotting.

	Composition
Transfer Buffer	25 mM Tris, 14.5 g/L Glycine, 20% (v/v) Ethanol, 2‰ SDS
TBST	10 mM Tris-HCl pH 8, 150 mM NaCl, 0.05% Tween 20
Hybridization Buffer	10 mM Tris-HCl pH 8, 150 mM NaCl, 0.05% Tween 20, 2% milk powder

5.18.6. Immunoblotting and electrochemiluminescence

In order to saturate non-specific binding sites, the membrane was incubated on a platform shaker at room temperature for 30 min in hybridization buffer.

The proteins were probed with a monoclonal anti-GFP (Roche Applied Science, catalogue no. 11 814 460 001), anti-Pma1 (De Craene, Soetens and André, 2001) or anti-yeast 3-phosphoglycerate kinase (anti-PGK) (Invitrogen) antibody. Hybridization with the primary antibody at 1:10,000 dilution was carried out for 1 h in hybridization buffer on a platform shaker and then the membrane was washed twice with hybridization buffer and once with TBST for 10 min.

Primary antibodies were detected with horseradish peroxidase-conjugated anti-mouse or anti-rabbit IgG secondary antibodies (GE Healthcare, catalogue no. NA931V). Secondary antibodies were left to hybridize for 45 min and the membrane was washed once with hybridization buffer and twice with TBST for 10 min to remove excess antibody.

Detection was performed with the Lumi-Light^{PLUS} enhanced chemiluminescence substrate (Roche) and CL-Xposure autoradiography film (Thermo Scientific). To this end, the membrane was dried of excess TBST, laid on ethanol dried glass and covered with 3 mL of substrate mixture for 3-5 min. Excess substrate was removed before covering with membrane wrap and development as per standard Western blotting procedure.

To allow detection of multiple proteins on a single membrane, the membrane was striped after every detection as follows: First, it was washed with TBST for 10 min and then incubated for 30 min in stripping solution at 50 °C under agitation. Finally, the same hybridization procedure was followed.

	Stripping Solution (50 mL)
10% (w/v) SDS	10 mL
Tris 1M pH6,8	3.125 mL
β-mercaptoethanol	350 µL
H_2O	36.5 mL

5.19. Epifluorescence Microscopy

For widefield and confocal epifluorescence microscopy, cells derived from exponentially growing early logarithmic phase liquid cultures were laid on a thin layer of 1% agarose (occasionally supplemented with the same substances/conditions used to treat the culture) and observed at room temperature by epifluorescence microscopy or at 29 °C by confocal microscopy.

Only the steady-state subcellular location of proteins was determined, by blocking neosynthesis with 3% glucose for 1.5 h before observation when expressed under the *GAL1* promoter.

To transiently induce expression of *pGAL1*- driven genes when needed, cells were first grown on raffinose (3%) and glucose (0.3%), then galactose (3%) was added for 3 hours, and finally glucose (3%) was provided to the cells 1.5 h before observation.

5.19.1. Widefield Epifluorescence microscopy

The endocytosis of GFP tagged proteins was evaluated by observation with an Eclipse 80i (Nikon), or an Eclipse E600 (Nikon) epifluorescence microscope equipped with a 100× differential interference contrast, NA 1.40 Plan-Apochromat objective (Nikon) and appropriate fluorescence light filter sets. Images were captured with a DS-Qi1Mc-U3 (Nikon), or a DXM1200 (Nikon) digital camera and NIS-Elements 4.3, or ACT-1 acquisition software (Nikon). Images were then autocorrected for optimal brightness and contrast, cropped, merged using the FIJI distribution (Schindelin *et al.*, 2012) of ImageJ (NIH), and annotated with Photoshop CC 2017 (Adobe Systems).

5.19.2. Confocal Laser Scanning Epifluorescence microscopy

Images were acquired with a Zeiss LSM710 microscope equipped with Airyscan (for some datasets) and a 100× differential interference contrast, NA 1.46 Alpha-Plan-Apochromat objective, with ZEN 2.1 SP2 software. GFP fluorescence was excited with the 488-nm line of the argon laser; mRFP, mCherry, and mKate2 fluorescence were excited with a 594-nm solid-state laser; mtagBFP2 fluorescence was excited with a 405-nm diode laser, and appropriate filters and beam splitters were used. Airyscan processing was performed with the ZEN software, using the default settings where appropriate. The final pixel size was 38.5 nm. The same laser intensities and other settings of the confocal microscope were used for all image acquisition. Images were then autocorrected for optimal brightness and contrast, cropped, merged using FIJI software, and annotated with Photoshop CC 2017. In each figure only a few cells representative of the whole cell population, observed in at least two independent biological replicate experiments, are shown.

5.20. Quantification of protein fluorescence

Confocal microscopy images were analyzed with a custom-made FIJI macro. The image of the EMC marker (Pil1) was processed first to create a mask of the EMCs. For each experiment, the better of the two following processing methods was used. (i) A 3 × 3 median filter (despeckle function) was applied, the ImageJ default thresholding method was applied, and then overlapping EMCs were separated using the watershed function. (ii) Alternatively, before default thresholding, the sharpen function and a Fourier space high-pass filter were applied, followed by the despeckle and dilate functions. After the EMC mask was obtained, the outlines of the focused cell surfaces were manually drawn with the ellipse tool, with the Can1, Gap1, or Nce102 image as a support for the user. The intensities of the channels of interest were measured both inside the complete cell outlines and in the EMC-positive area. The median of the fluorescence intensity in the whole image was used as a measure of the background. The tendency of the protein of interest to localize to the EMCs was measured as the ratio of the background-corrected mean intensity per pixel of the EMC area to that of the area delimited by the whole-cell outline and excluding the EMC area. The Pearson's correlation coefficient was determined using a custom-made macro based on the coloc2 plugin of FIJI. All parameters were calculated from at least two independent biological replicates for each condition. The values for single cells are presented in box-and-whisker plots. After confirming statistically that the two independent biological replicates gave statistically nonsignificant differences in mean values, the values of the two independent experiments were merged.

5.21. Statistical Analysis of Quantifications

Cell fluorescence measurements were imported to GraphPad Prism software and one way-ANOVA with the nonparametric Kruskal–Wallis test, and Dunn's multiple-comparison post hoc analyses were used to assess the significance of the value differences of all measurements. Quantification figures were edited in Illustrator CC 2018 (Adobe Systems) and presented in Photoshop CC 2017 along corresponding representative cell images.

6. References

Athanasopoulos, A. *et al.* (2013) “Eisosome distribution and localization in the meiotic progeny of Aspergillus nidulans,” *Fungal Genetics and Biology*, 53, pp. 84–96. doi: 10.1016/j.fgb.2013.01.002.

Bagatolli, L. A. *et al.* (2010) “An outlook on organization of lipids in membranes: Searching for a realistic connection with the organization of biological membranes,” *Progress in Lipid Research*, 49(4), pp. 378–389. doi: 10.1016/j.plipres.2010.05.001.

Berchtold, D. *et al.* (2012) “Plasma membrane stress induces relocalization of Slm proteins and activation of TORC2 to promote sphingolipid synthesis,” *Nat Cell Biol*, 14(5), pp. 542–547. doi: 10.1038/ncb2480.

Berchtold, D. and Walther, T. C. (2009) “TORC2 Plasma Membrane Localization Is Essential for Cell Viability and Restricted to a Distinct Domain,” *Molecular Biology of the Cell*, 20(5), pp. 1565–1575. doi: 10.1091/mbc.E08-10-1001.

Bianchi, F. *et al.* (2018) “Steric exclusion and protein conformation determine the localization of plasma membrane transporters,” *Nature Communications*, 9(1), pp. 1–30. doi: 10.1038/s41467-018-02864-2.

Bonneaud, N. *et al.* (1991) “A family of low and high copy replicative, integrative and single-stranded S. cerevisiae/E. coli shuttle vectors,” *Yeast*, 7(6), pp. 609-15. doi: 10.1002/yea.320070609.

Brach, T., Specht, T. and Kaksonen, M. (2011) “Reassessment of the role of plasma membrane domains in the regulation of vesicular traffic in yeast,” *Journal of Cell Science*, 124(3), pp. 328–337. doi: 10.1242/jcs.078519.

Breslow, D. K. *et al.* (2010) “Orm family proteins mediate sphingolipid homeostasis,” *Nature*, 463(7284), pp. 1048–1053. doi: 10.1038/nature08787.

Contreras, F. X. *et al.* (2012) “Molecular recognition of a single sphingolipid species by a protein’s transmembrane domain,” *Nature*, 481(7382), pp. 525–529. doi: 10.1038/nature10742.

Curthoys, N., M. *et al.* (2015) *Dances with Membranes: Breakthroughs from Super-resolution Imaging*. *Lipid Domains*. *Curr Top Membr*. 75, pp. 59-123. doi: 10.1016/bs.ctm.2015.03.008.

De Craene, J. O., Soetens, O. and André, B. (2001) “The Npr1 Kinase Controls Biosynthetic and Endocytic Sorting of the Yeast Gap1 Permease,” *Journal of Biological Chemistry*, 276(47), pp. 43939–43948. doi: 10.1074/jbc.M102944200.

Crapeau, M., Merhi, A. and André, B. (2014) “Stress conditions promote yeast Gap1 permease ubiquitylation and down-regulation via the arrestin-like bul and aly proteins,” *Journal of Biological Chemistry*, 289(32), pp. 22103–22116. doi: 10.1074/jbc.M114.582320.

Diallinas, G. (2008) “Biochemistry: An almost-complete movie,” *Science*, pp. 1644–1645. doi: 10.1126/science.1168107.

Didion, T. *et al.* (1998) “The permease homologue Ssy1p controls the expression of amino acid and peptide transporter genes in Saccharomyces cerevisiae,” *Molecular Microbiology*, 27(3), pp. 643–650. doi: 10.1046/j.1365-2958.1998.00714.x.

Donaton, M. C. V. *et al.* (2003) "The Gap1 general amino acid permease acts as an amino acid sensor for activation of protein kinase A targets in the yeast Saccharomyces cerevisiae," *Molecular Microbiology*, 50(3), pp. 911–929. doi: 10.1046/j.1365-2958.2003.03732.x.

Ejsing, C. S. *et al.* (2009) "Global analysis of the yeast lipidome by quantitative shotgun mass spectrometry," *Proceedings of the National Academy of Sciences*, 106(7), pp. 2136–2141. doi: 10.1073/pnas.0811700106.

Foderaro, J. E., Douglas, L. M. and Konopka, J. B. (2017) "MCC / Eisosomes Regulate Cell Wall Synthesis and Stress Responses in Fungi," *Journal of Fungi*, 3(61), pp. 1–18. doi: 10.3390/jof3040061.

Fröhlich, F. *et al.* (2009) "A genome-wide screen for genes affecting eisosomes reveals Nce102 function in sphingolipid signaling," *Journal of Cell Biology*, 185(7), pp. 1227–1242. doi: 10.1083/jcb.200811081.

Gao, X. *et al.* (2010) "Mechanism of substrate recognition and transport by an amino acid antiporter," *Nature*, 463(7282), pp. 828–832. doi: 10.1038/nature08741.

Ghaddar, K., Krammer, E.-M., *et al.* (2014) "Converting the yeast arginine Can1 permease to a lysine permease," *Journal of Biological Chemistry*, 289(10), pp. 7232–7246. doi: 10.1074/jbc.M113.525915.

Ghaddar, K., Merhi, A., *et al.* (2014) "Substrate-Induced Ubiquitylation and Endocytosis of Yeast Amino Acid Permeases," *Molecular and Cellular Biology*, 34(24), pp. 4447–4463. doi: 10.1128/MCB.00699-14.

Gietz, R. D. and Schiestl, R. H. (2007) "Quick and easy yeast transformation using the LiAc/SS carrier DNA/PEG method," *Nature Protocols*, 2(1), pp. 35–37. doi: 10.1038/nprot.2007.14.

Gournas, C. *et al.* (2015) "The Aspergillus nidulans proline permease as a model for understanding the factors determining substrate binding and specificity of fungal amino acid transporters.," *The Journal of biological chemistry*, 290(10), pp. 6141–6155. doi: 10.1074/jbc.M114.612069.

Gournas, C. *et al.* (2017) "Transition of yeast Can1 transporter to the inward-facing state unveils an α-arrestin target sequence promoting its ubiquitylation and endocytosis," *Molecular Biology of the Cell*, 28(21), p. mbc.E17--02--0104. doi: 10.1091/mbc.E17-02-0104.

Gournas, C. *et al.* (2018) "Conformation-dependent partitioning of yeast nutrient transporters into starvation-protective membrane domains," *Proceedings of the National Academy of Sciences*, 115(14), pp. E3145–E3154. doi: 10.1073/pnas.1719462115.

Grenson, M. *et al.* (1966) "Multiplicity of the amino acid permeases in Saccharomyces cerevisiae," *Biochimica et Biophysica Acta (BBA) - General Subjects*, 127(2), pp. 325–338. doi: 10.1016/0304-4165(66)90387-4.

Grossmann, G. *et al.* (2007) "Membrane potential governs lateral segregation of plasma membrane proteins and lipids in yeast," *The EMBO Journal*, 26(1), pp. 1–8. doi: 10.1038/sj.emboj.7601466.

Grossmann, G. *et al.* (2008) "Plasma membrane microdomains regulate turnover of transport proteins in yeast," *Journal of Cell Biology*, 183(6), pp. 1075–1088. doi: 10.1083/jcb.200806035.

Grousl, T. *et al.* (2015) “Evolutionarily conserved 5’-3’ exoribonuclease Xrn1 accumulates at plasma membrane-associated eisosomes in post-diauxic yeast,” *PLoS ONE*, 10(3). doi: 10.1371/journal.pone.0122770.

Guan, X. L. *et al.* (2010) *Yeast lipid analysis and quantification by mass spectrometry*. 2nd ed, *Methods in Enzymology*. 2nd ed. Elsevier Inc. doi: 10.1016/S0076-6879(10)70015-X.

Güldener, U. *et al.* (1996) “A new efficient gene disruption cassette for repeated use in budding yeast,” *Nucleic Acids Res*, 24(13), pp. 2519–2524. Available at: http://www.ncbi.nlm.nih.gov/pubmed/8692690.

Han, X., Yang, K. and Gross, R. W. (2012) “Multi-dimensional mass spectrometry-based shotgun lipidomics and novel strategies for lipidomic analyses,” *Mass Spectrometry Reviews*, 31(1), pp. 134–178. doi: 10.1002/mas.20342.

Hanada, K. *et al.* (1995) “Both Sphingolipids and Cholesterol Participate in the Detergent Insolubility of Alkaline Phosphatase, a Glycosylphosphatidylinositol-anchored Protein, in Mammalian Membranes,” *Journal of Biological Chemistry*, 270(11), pp. 6254–6260. doi: 10.1074/jbc.270.11.6254.

Hein, C. *et al.* (1995) “NPI1, an essential yeast gene involved in induced degradation of Gap1 and Fur4 permeases, encodes the Rsp5 ubiquitin—protein ligase,” *Molecular Microbiology*, 18(1), pp. 77–87. doi: 10.1111/j.1365-2958.1995.mmi_18010077.x.

Huh, W. *et al.* (2003) “Global analysis of protein localization in budding yeast,” *Nature*, 425(6959), pp. 686–691. doi: 10.1038/nature02026.

Iraqui, I. *et al.* (1999) “Amino Acid Signaling in Saccharomyces cerevisiae : a Permease-Like Sensor of External Amino Acids and F-Box Protein Grr1p Are Required for Transcriptional Induction of the AGP1 Gene, Which Encodes a Broad-Specificity Amino Acid Permease,” *Molecular and Cellular Biology*, 19(2), pp. 989–1001. doi: 10.1128/MCB.19.2.989.

Jacobs, P., Jauniaux, J.-C. and Grenson, M. (1980) “A cis-dominant regulatory mutation linked to the argB-argC gene cluster in Saccharomyces cerevisiae,” *Journal of Molecular Biology*, 139(4), pp. 691–704. doi: 10.1016/0022-2836(80)90055-8.

Janke, C. *et al.* (2004) “A versatile toolbox for PCR-based tagging of yeast genes: New fluorescent proteins, more markers and promoter substitution cassettes,” *Yeast*, 21(11), pp. 947–962. doi: 10.1002/yea.1142.

Jardetzky, O. (1966) “Simple allosteric model for membrane pumps.,” *Nature*, 211(5052), pp. 969–70.

Kabeche, R., Howard, L. and Moseley, J. B. (2015) “Eisosomes provide membrane reservoirs for rapid expansion of the yeast plasma membrane.,” *Journal of cell science*, pp. 4057–4062. doi: 10.1242/jcs.176867.

Karotki, L. *et al.* (2011) “Eisosome proteins assemble into a membrane scaffold,” *Journal of Cell Biology*, 195(5), pp. 889–902. doi: 10.1083/jcb.201104040.

Klasson, H., Fink, G. R. and Ljungdahl, P. O. (1999) “Ssy1p and Ptr3p Are Plasma Membrane Components of a Yeast System That Senses Extracellular Amino Acids,” *Molecular and Cellular Biology*, 19(8), pp. 5405–5416. doi: 10.1128/MCB.19.8.5405.

Klose, C. *et al.* (2010) “Yeast lipids can phase-separate into micrometer-scale membrane domains,” *Journal of Biological Chemistry*, 285(39), pp. 30224–30232. doi: 10.1074/jbc.M110.123554.

Kodama, Y. *et al.* (2002) “Genome-wide expression analysis of genes affected by amino acid sensor Ssy1p in Saccharomyces cerevisiae,” *Current Genetics*, 41(2), pp. 63–72. doi: 10.1007/s00294-002-0291-1.

Krishnamurthy, H. and Gouaux, E. (2012) “X-ray structures of LeuT in substrate-free outward-open and apo inward-open states,” *Nature*, 481(7382), pp. 469–474. doi: 10.1038/nature10737.

Kusumi, A. *et al.* (2011) “Hierarchical mesoscale domain organization of the plasma membrane,” *Trends in Biochemical Sciences*. Elsevier Ltd, pp. 604–615. doi: 10.1016/j.tibs.2011.08.001.

Lauwers, E., Grossmann, G. and André, B. (2007) “Evidence for Coupled Biogenesis of Yeast Gap1 Permease and Sphingolipids: Essential Role in Transport Activity and Normal Control by Ubiquitination,” *Molecular Biology of the Cell*, 18(8), pp. 3068–3080. doi: 10.1091/mbc.e07-03-0196.

Lingwood, D. and Simons, K. (2009) “Lipid Rafts As a Membrane-Organizing Principle,” *Science*, 327(5961), p. 46 LP-- 50. Available at: http://science.sciencemag.org/content/327/5961/46.abstract.

Loibl, M. *et al.* (2010) “C terminus of Nce 102 determines the structure and function of microdomains in the Saccharomyces cerevisiae plasma membrane,” *Eukaryotic Cell*, 9(8), pp. 1184–1192. doi: 10.1128/EC.00006-10.

Löoke, M., Kristjuahan, K. and Kristjuhan, A. (2011) “Extraction of Genomic Dna From Yeasts for Pcr- Based Applications,” *Biotechniques*, 50(5), pp. 325–328. doi: 10.2144/000113672.EXTRACTION.

Lorent, J. H. *et al.* (2017) “Structural determinants and functional consequences of protein affinity for membrane rafts,” *Nature Communications*. Springer US, 8(1). doi: 10.1038/s41467-017-01328-3.

Luo, G. *et al.* (2008) “The sphingolipid long-chain base-Pkh1/2-Ypk1/2 signaling pathway regulates eisosome assembly and turnover,” *Journal of Biological Chemistry*, 283(16), pp. 10433–10444. doi: 10.1074/jbc.M709972200.

Malínská, K. *et al.* (2003) “Visualization of Protein Compartmentation within the Plasma Membrane of Living Yeast Cells,” *Molecular Biology of the Cell*, 14(11), pp. 4427–4436. doi: 10.1091/mbc.E03-04-0221.

Malínská, K. *et al.* (2004) “Distribution of Can1p into stable domains reflects lateral protein segregation within the plasma membrane of living S. cerevisiae cells,” *Journal of Cell Science*, 117(25), pp. 6031–6041. doi: 10.1242/jcs.01493.

Merhi, A. and André, B. (2012) “Internal Amino Acids Promote Gap1 Permease Ubiquitylation via TORC1/Npr1/14-3-3-Dependent Control of the Bul Arrestin-Like Adaptors,” *Molecular and Cellular Biology*, 32(22), pp. 4510–4522. doi: 10.1128/MCB.00463-12.

Mollinedo, F. (2012) “Lipid raft involvement in yeast cell growth and death,” *Frontiers in Oncology*, 2(October), pp. 1–15. doi: 10.3389/fonc.2012.00140.

Moor, H. and Mühlethaler, K. (1963) “Fine structure in frozen-etched yeast cells,” *Journal of Cell Biology*, 17, pp. 609–28.

Moreira, K. E. *et al.* (2008) “Pil1 Controls Eisosome Biogenesis,” *Molecular Biology of the Cell*, 20(3), pp. 809–818. doi: 10.1091/mbc.E08-03-0313.

Moreira, K. E. *et al.* (2012) “Seg 1 controls eisosome assembly and shape,” *Journal of Cell Biology*, 198(3), pp. 405–420. doi: 10.1083/jcb.201202097.

Müller, N. S., Wedlich-Söldner, R. and Spira, F. (2012) “From mosaic to patchwork: Matching lipids and proteins in membrane organization,” *Molecular Membrane Biology*, 29(5), pp. 186–196. doi: 10.3109/09687688.2012.687461.

Nagiec, M. M. *et al.* (1994) “The LCB2 gene of Saccharomyces and the related LCB1 gene encode subunits of serine palmitoyltransferase, the initial enzyme in sphingolipid synthesis.,” *Proceedings of the National Academy of Sciences of the United States of America*, 91(17), pp. 7899–902. doi: 10.1073/pnas.91.17.7899.

Nikko, E., Marini, A. and André, B. (2007) “Permease Recycling and Ubiquitination Status Reveal a Particular Role for Bro1 in the Multivesicular Body Pathway,” *Journal of Biological Chemistry*, 278(50), pp. 50732-43. doi: 10.1074/jbc.M306953200.

Olivera-Couto, A. *et al.* (2011) “The eisosome core is composed of BAR domain proteins,” *Molecular Biology of the Cell*, 22(13), pp. 2360–2372. doi: 10.1091/mbc.E10-12-1021.

Olivera-Couto, A. *et al.* (2015) “Eisosomes are dynamic plasma membrane domains showing Pil1-Lsp1 heteroligomer binding equilibrium,” *Biophysical Journal*, 108(7), pp. 1633–1644. doi: 10.1016/j.bpj.2015.02.011.

Opekarová, M., Robl, I. and Tanner, W. (2002) “Phosphatidyl ethanolamine is essential for targeting the arginine transporter Can1p to the plasma membrane of yeast,” *Biochimica et Biophysica Acta - Biomembranes*, 1564(1), pp. 9–13. doi: 10.1016/S0005-2736(02)00455-8.

Popov-Čeleketić, D. *et al.* (2016) “A plasma membrane association module in yeast amino acid transporters,” *Journal of Biological Chemistry*, 291(31), pp. 16024–16037. doi: 10.1074/jbc.M115.706770.

Regenberg, B. and Kielland-Brandt, M. C. (2001) “Amino acid residues important for substrate specificity of the amino acid permeases Can1p and Gnp1p in Saccharomyces cerevisiae.,” *Yeast*, 18(15), pp. 1429–1440. doi: 10.1002/yea.792.

Roelants, F. M. *et al.* (2011) “Protein kinase Ypk1 phosphorylates regulatory proteins Orm1 and Orm2 to control sphingolipid homeostasis in Saccharomyces cerevisiae,” *Proceedings of the National Academy of Sciences*, 108(48), pp. 19222–19227. doi: 10.1073/pnas.1116948108.

Rothbauer, U. *et al.* (2008) “A Versatile Nanotrap for Biochemical and Functional Studies with Fluorescent Fusion Proteins,” *Molecular & Cellular Proteomics*, 7(2), pp. 282–289. doi: 10.1074/mcp.M700342-MCP200.

Saliba, A.-E., Vonkova, I. and Gavin, A.-C. (2015) “The systematic analysis of protein–lipid interactions comes of age,” *Nature Reviews Molecular Cell Biology*, 16(12), pp. 753–761. doi: 10.1038/nrm4080.

Schindelin, J. *et al.* (2012) “Fiji: an open-source platform for biological-image analysis,” *Nat Meth*, 9(7), pp. 676–682. Available at: http://dx.doi.org/10.1038/nmeth.2019.

Schröder, R., London, E. and Brown, D. (1994) “Interactions between saturated acyl chains confer detergent resistance on lipids and glycosylphosphatidylinositol (GPI)-anchored proteins: GPI-anchored proteins in liposomes and cells show similar behavior.,” *Proceedings of the National Academy of Sciences of the United States of America*, 91(25), pp. 12130–12134.

Schumacher, D. *et al.* (2018) “Nanobodies: Chemical Functionalization Strategies and Intracellular Applications,” *Angewandte Chemie - International Edition*, 57(9), pp. 2314–2333. doi: 10.1002/anie.201708459.

Séron, K. *et al.* (1999) “Uracil-induced down-regulation of the yeast uracil permease,” *Journal of Bacteriology*, 181(6), pp. 1793–1800. doi: .

Serrano, R., Kiellandbrandt, M. C. and Fink, G. R. (1986) “Yeast Plasma-Membrane Atpase Is Essential for Growth and Has Homology with (Na++K+), K+- and Ca-2+-Atpases,” *Nature*, 319(6055), pp. 689–693. doi: 10.1038/319689a0.

Simons, K. and Ikonen, E. (1997) “Functional rafts in cell membranes,” *Nature*, 387(6633), pp. 569–572. doi: 10.1038/42408.

Singer, S. J. and Nicolson, G. L. (1972) “The fluid mosaic model of the structure of cell membranes.,” *Science*, pp. 720–731. doi: 10.1017/CBO9781107415324.004.

Spira, F. *et al.* (2012) “Patchwork organization of the yeast plasma membrane into numerous coexisting domains,” *Nature Cell Biology*, 14(6), pp. 640–648. doi: 10.1038/ncb2487.

Strádalová, V. *et al.* (2009) “Furrow-like invaginations of the yeast plasma membrane correspond to membrane compartment of Can1,” *Journal of Cell Science*, 122(16), pp. 2887–2894. doi: 10.1242/jcs.051227.

Strádalová, V. *et al.* (2012) “Distribution of cortical endoplasmic reticulum determines positioning of endocytic events in yeast plasma membrane,” *PLoS ONE*, 7(4). doi: 10.1371/journal.pone.0035132.

Takeo, K., Shigeta, M. and Takagi, Y. (1976) “Plasma membrane ultrastructural differences between the exponential and stationary phases of Saccharomyces cerevisiae as revealed by freeze-etching,” *Journal of General Microbiology*, 97(2), pp. 323–329. doi: 10.1099/00221287-97-2-323.

Vangelatos, I. *et al.* (2009) “Modelling and mutational evidence identify the substrate binding site and functional elements in APC amino acid transporters.,” *Molecular membrane biology*, 26(5), pp. 356–370. doi: 10.1080/09687680903170546.

Vaškovičová, K. *et al.* (2017) “MRNA decay is regulated via sequestration of the conserved 5’-3’ exoribonuclease Xrn1 at eisosome in yeast,” *European Journal of Cell Biology*, pp. 591–599. doi: 10.1016/j.ejcb.2017.05.001.

Villers, J. *et al.* (2017) “Study of the Plasma Membrane Proteome Dynamics Reveals Novel Targets of the Nitrogen Regulation in Yeast,” *Molecular & Cellular Proteomics*, 16(9), pp. 1652–1668. doi: 10.1074/mcp.M116.064923.

Volland, C. *et al.* (1994) “Endocytosis and degradation of the yeast uracil permease under adverse conditions,” *Journal of Biological Chemistry*, 269(13), pp. 9833–9841.

Walther, P., Müller, M. and Schweingruber, M. E. (1984) “The ultrastructure of the cell surface and plasma membrane of exponential and stationary phase cells of Schizosaccharomyces pombe, grown in different media,” *Archives of Microbiology*, 137, pp. 128–134.

Walther, T. C. *et al.* (2006) “Eisosomes mark static sites of endocytosis,” *Nature*, 439(7079), pp. 998–1003. doi: 10.1038/nature04472.

Walther, T. C. *et al.* (2007) “Pkh-kinases control eisosome assembly and organization.,” *The EMBO journal*, 26(24), pp. 4946–4955. doi: 10.1038/sj.emboj.7601933.

Wedlich-Söldner, R. *et al.* (2018) “Lateral plasma membrane compartmentalization links protein function and turnover,” *bioRxiv*, p. 285510. doi: 10.1101/285510.

Wenk, M. R. (2010) “Lipidomics: New tools and applications,” *Cell*. Elsevier Inc., 143(6), pp. 888–895. doi: 10.1016/j.cell.2010.11.033.

Yamashita, A. *et al.* (2005) “Crystal structure of a bacterial homologue of Na+/Cl--dependent neurotransmitter transporters,” *Nature*, 437(7056), pp. 215–223. doi: 10.1038/nature03978.

Yoshikawa, K. *et al.* (2009) “Comprehensive phenotypic analysis for identification of genes affecting growth under ethanol stress in Saccharomyces cerevisiae,” *FEMS Yeast Research*, 9(1), pp. 32–44. doi: 10.1111/j.1567-1364.2008.00456.x.

Young, M. E. *et al.* (2002) “The Sur7p family defines novel cortical domains in Saccharomyces cerevisiae, affects sphingolipid metabolism, and is involved in sporulation.,” *Molecular and cellular biology*, 22(3), pp. 927–934. doi: 10.1128/MCB.22.3.927-934.2002.

Yu, J. H. *et al.* (2004) “Double-joint PCR: A PCR-based molecular tool for gene manipulations in filamentous fungi,” *Fungal Genetics and Biology*, 41(11), pp. 973–981. doi: 10.1016/j.fgb.2004.08.001.

Zeppelin, T. *et al.* (2018) “A direct interaction of cholesterol with the dopamine transporter prevents its out-to-inward transition,” *PLOS Computational Biology*. Edited by A. MacKerell, 14(1), p. e1005907. doi: 10.1371/journal.pcbi.1005907.